NUREG/CR-0609
TREE-1331
for the U.S. Nuclear Regulatory Commission

POWER-COOLING-MISMATCH TEST SERIES FUEL ROD MATERIAL PROPERTIES DATA REPORT

DEBORAH K. KERWIN ADRIENNE H. NOVICK
CHARLES S. OLSEN

May 1979

EG&G Idaho, Inc.

IDAHO NATIONAL ENGINEERING LABORATORY

DEPARTMENT OF ENERGY

IDAHO OPERATIONS OFFICE UNDER CONTRACT EY-76-C-07-1570

Available from
National Technical Information Service
Springfield, Virginia 22161
Price: Printed Copy A05; Microfiche $3.00

The price of this document for requesters outside the North American continent can be obtained from the National Technical Information Service.

NUREG/CR-0609
TREE-1331
R3

POWER-COOLING-MISMATCH TEST SERIES FUEL ROD MATERIAL PROPERTIES DATA REPORT

Deborah K. Kerwin
Adrienne H. Novick
Charles S. Olsen

EG&G Idaho, Inc.
Idaho Falls, Idaho 83401

Published May 1979

PREPARED FOR THE
U.S. NUCLEAR REGULATORY COMMISSION
AND THE U. S. DEPARTMENT OF ENERGY
IDAHO OPERATIONS OFFICE
UNDER CONTRACT NO. EY-76-C-07-1570
NRC FIN NO. A6041

ACKNOWLEDGMENTS

The authors extend special thanks to Dr. H. M. Chung, Material Science Division of the Argonne National Laboratory in Argonne, Illinois, for performing the out-of-reactor transient burst tests of representative samples of power-cooling-mismatch cladding, and for providing much of the information contained in the cladding burst characteristics section.

ABSTRACT

The physical, chemical, mechanical, and metallurgical properties of the Power-Cooling-Mismatch (PCM) Test Series fuel rod components are presented. These data were obtained from examinations and tests of representative unirradiated fuel rod materials, and are necessary to understand and evaluate both fuel rod behavior during irradiation testing in the PCM Test Series, and the posttest conditions of the various fuel rod materials.

SUMMARY

Nondestructive and destructive examinations and tests were performed on representative unirradiated Power-Cooling-Mismatch (PCM) Test Series fuel rod components to characterize the component material properties. The examination and test results are necessary to understand and evaluate both fuel rod behavior during irradiation testing in the PCM Test Series, and the posttest conditions of the various fuel rod materials. Characterization of the cladding included physical dimensions, chemical analysis, uniaxial tensile properties, burst characteristics, microstructure, crystallographic texture, and hydride orientation. Fuel characterization for each of three enrichments included sintering conditions, physical dimensions, chemical analysis, microstructure, and density. End cap characterization included chemical analysis, and tensile properties and hardness. Alumina spacer characterization included physical dimensions; chemical analysis; porosity and absorption; and density, compressive strength, and hardness. Compression spring characterization included physical dimensions, chemical analysis, and tensile strength.

CONTENTS

FIGURES

TABLES

778 191

POWER-COOLING-MISMATCH TEST SERIES FUEL ROD MATERIAL PROPERTIES DATA REPORT

I. INTRODUCTION

The Power-Cooling-Mismatch (PCM) Test Series experiments are being conducted by the Thermal Fuels Behavior Program of EG&G Idaho, Inc., as part of the Nuclear Regulatory Commission's Water Reactor Safety Research Fuel Behavior Program[1]. These tests are being performed in the Power Burst Facility reactor to characterize the behavior of previously unirradiated pressurized water reactor type fuel rods at power densities and flow conditions ranging from normal to stable film boiling operating conditions. The PCM Test Series is directed toward providing experimental data for assessment of analytical models developed to predict the behavior of light water reactor fuels under normal and postulated accident conditions.

This report contains data on the physical, chemical, mechanical, and metallurgical properties of the cladding, fuel, end cap, alumina spacer, and compression spring materials used in fabricating the PCM Test Series unirradiated fuel rods. These data were obtained from examinations and tests of representative fuel rod materials, and are necessary to understand and evaluate both the fuel rod behavior during irradiation testing in the PCM Test Series, and the posttest conditions of the various fuel rod materials.

Ninety PCM Test Series fuel rods were fabricated by Gulf United Nuclear Fuels Corporation[a]. The individual rod components were manufactured by the following vendors: zircaloy-4 cladding tubing, Westinghouse Electric Corporation; UO_2 fuel pellets, Gulf United Nuclear Fuels Corporation, Chemical Operations; zircaloy-2 end cap rod stock, Wah Chang Albany Corporation; alumina spacers, Coors/Spectro-Chemical Laboratory; and compression spring wire, New England High Carbon Wire Corporation. Figure 1 gives an overall view of the fuel rod and Figure 2 presents each of the five fuel rod components in detail.

---

[a] Gulf United Nuclear Fuels Corporation, Fabrications Operations, P.O. Box 605, New Haven, Connecticut 06503.

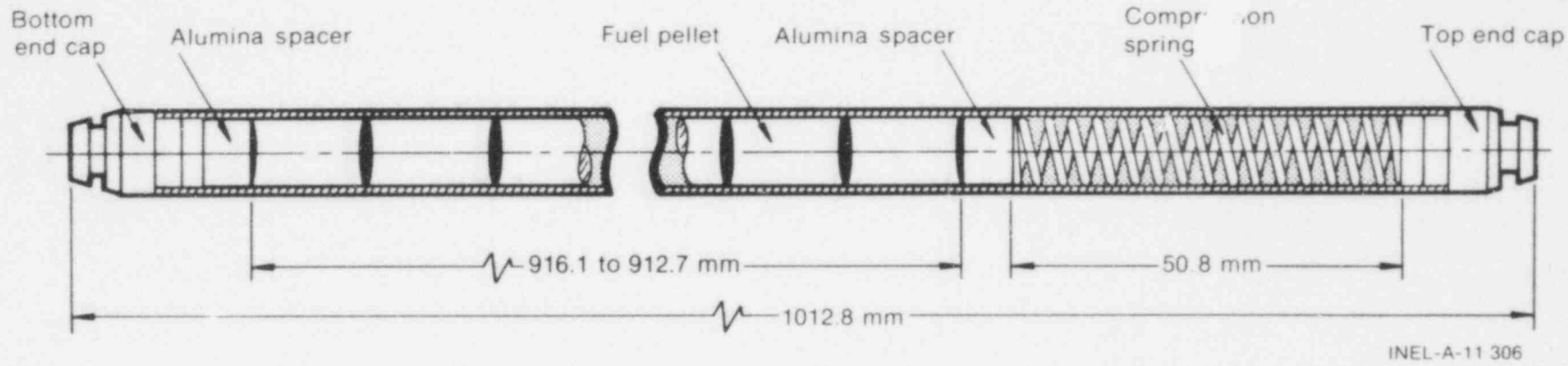

Fig. 1 Schematic of PCM fuel rod.

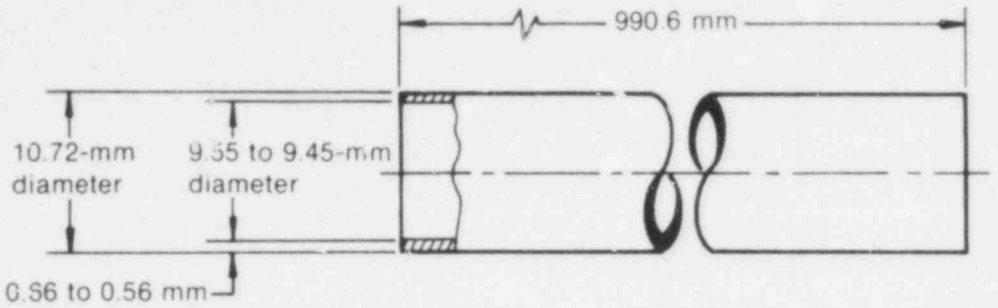

a. Cladding tube

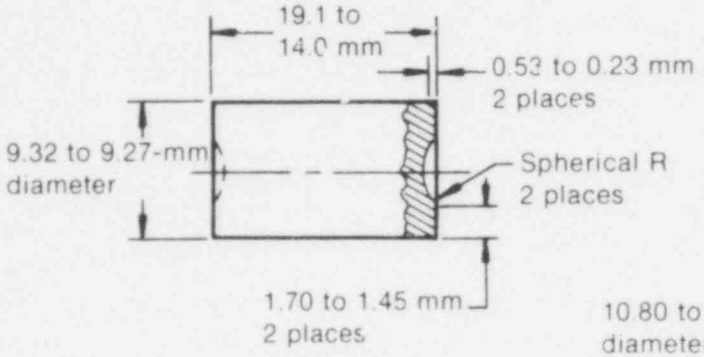

b. Fuel pellet

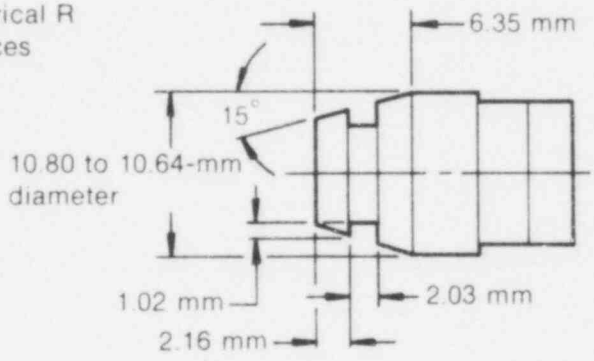

c. Top and bottom end caps

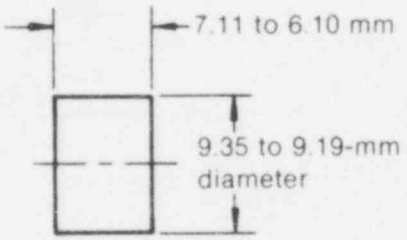

d. Alumina spacer

Wire diameter	1.02 mm
Outside diameter	9.02 mm
Free length	60.33 mm
Solid height	20.32 mm maximum
Spring rate	1121 to 1523 N/m
Type of ends	Squared and ground
Protective finish	None
Direction of wind	Optional
No. of active coils	15
No. of total coils	17

e. Compression spring specifications

INEL-A-11 305

Fig. 2 PCM fuel rod component details.

778 19

II. CLADDING CHARACTERIZATION

The PCM fuel rod cladding was made from zircaloy-4 tubing (heat number 384956) manufactured by Westinghouse Electric Corporation[a] according to ASTM B353-69 specifications. The tubing manufacturing requirements specified that the tubing be made from ingots by multiple vacuum melting in arc furnaces, cold worked a minimum of 50%, and stress-relieved. The following sections discuss cladding dimensions, chemical analysis, tensile properties, burst characteristics, microstructure, crystallographic texture, and hydride orientation.

1. PHYSICAL DIMENSIONS

The cladding nominal dimensions were 10.72-mm outside diameter, 9.50-mm inside diameter, and 0.61-mm wall thickness. Three circumferential stylus traces of an approximately 0.30-m piece of cladding were made to determine the ovality and out-of-roundness of the cladding. The traces are shown in Figure 3. Very little ovality is evident. A measure of the cladding out-of-roundness is the difference between the largest radius circle that will fit completely inside the trace, and the smallest circle that will contain the trace. This difference is 5.1 μm in Figure 3(a), and 6.4 μm in Figures 3(b) and 3(c).

[a] Westinghouse Electric Corporation, R.D. #2, Box 45, Blairsville, Pennsylvania 15717.

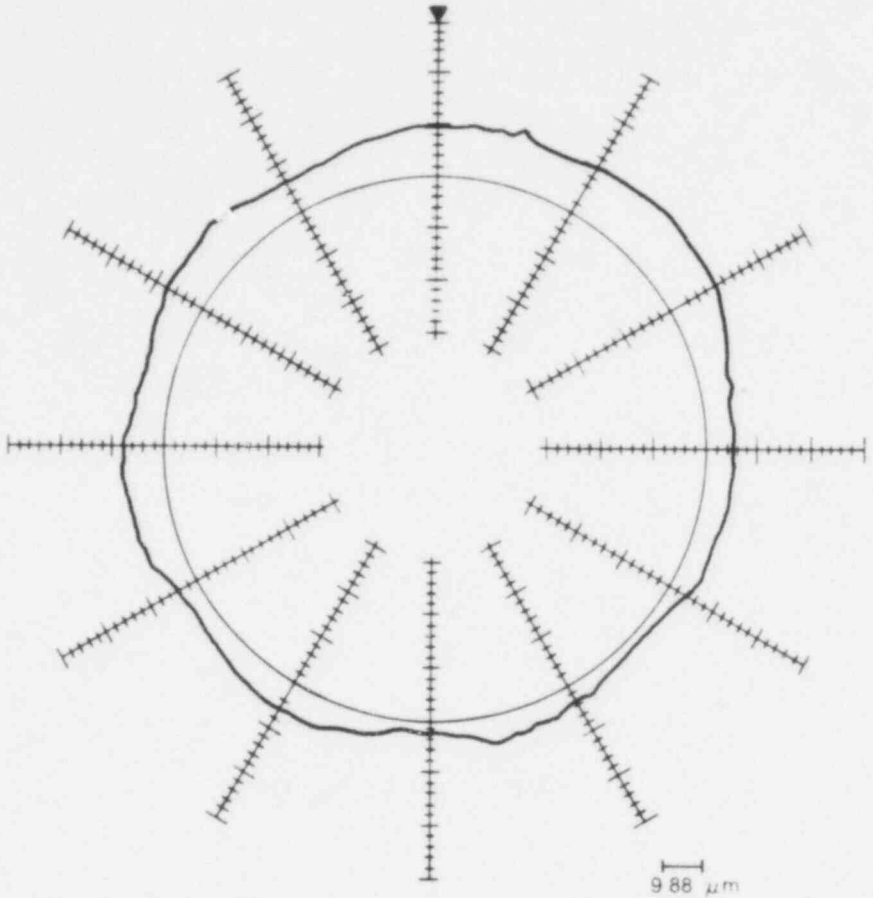

a Ovality stylus trace at one end of a 0.3-m piece of cladding tubing

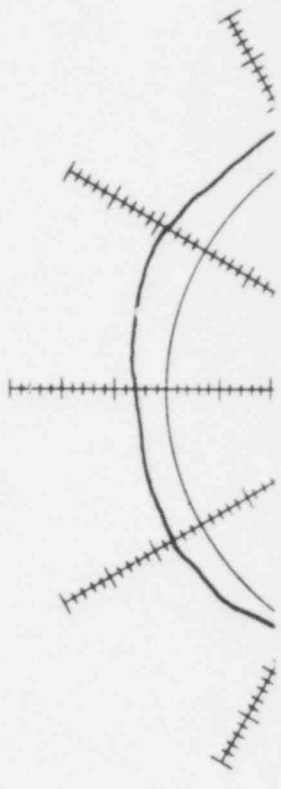

b Ovality stylus trac

Fig. 3 Ovality stylus traces at t

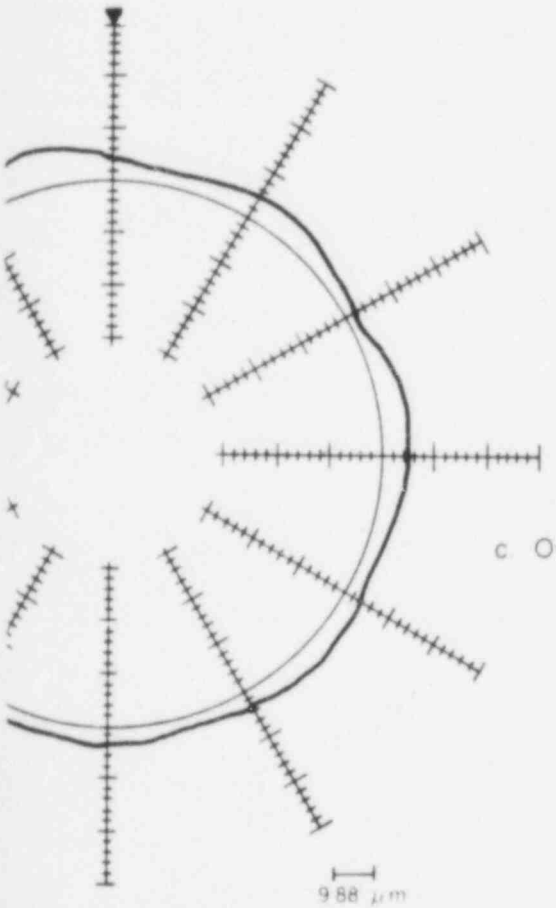

center of a 0.3-m piece of cladding tubing

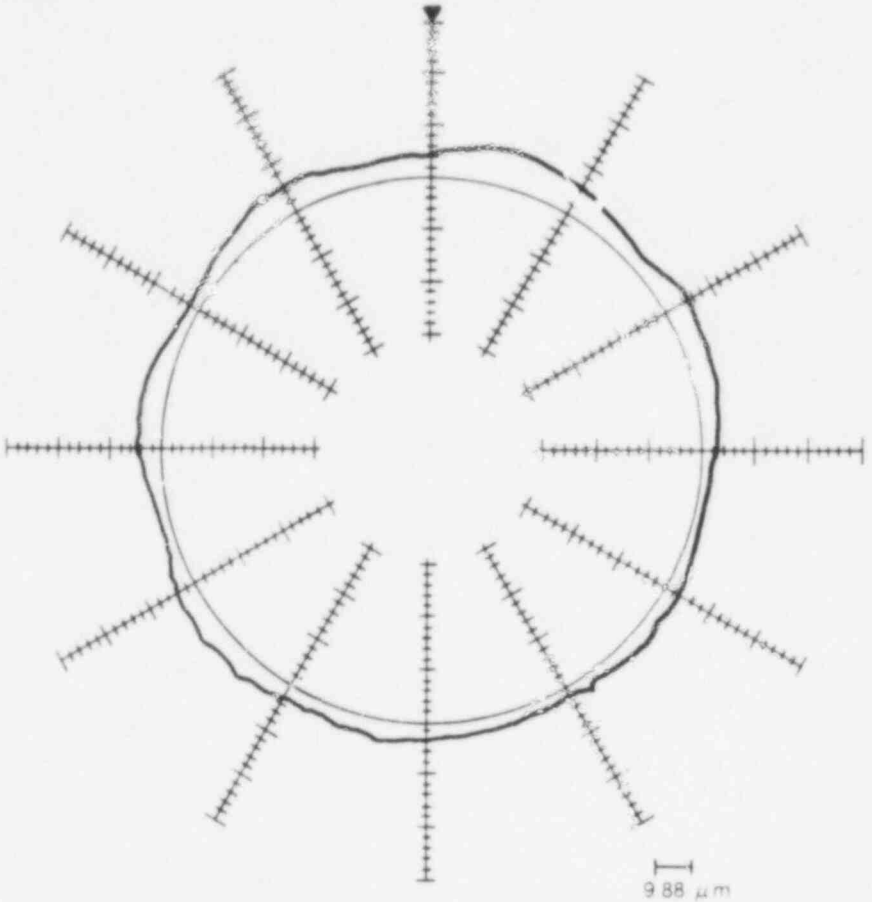

c. Ovality stylus trace at the other end of a 0.3-m piece of cladding tubing

INEL-B-11 295

xial elevations of a 0.3-m piece of PCM cladding tubing.

2. CHEMICAL ANALYSIS

Chemical analyses of the zircaloy-4 ingot and cladding tubing were supplied by the tubing manufacturer (Westinghouse Electric Corporation) and are given in Tables I and II, respectively. Table III presents the tubing chemical analysis performed by the fuel rod manufacturer (Gulf United Nuclear Fuels Corporation). The oxygen content was specified to be less than 1400 ppm. The chemical composition and impurity levels are within the specified ranges.

TABLE I

ZIRCALOY-4 CLADDING TUBING INGOT ANALYSIS PERFORMED BY TUBING MANUFACTURER

	Composition (%)			
	Specification	Top	Middle	Bottom
Sn	1.20 to 1.70	1.52	1.48	1.42
Fe	0.18 to 0.24	0.22	0.20	0.22
Cr	0.07 to 0.13	0.12	0.11	0.11
Fe+Cr	0.28 to 0.37	0.34	0.31	0.33
	Impurities (ppm)			
Al	<75	39	45	34
B	<0.5	<0.2	<0.2	<0.2
C	<270	120	140	140
Cd	<0.5	<0.2	<0.2	<0.2
Cl	<20	<5	<5	<5
Co	<20	<10	<10	<10
Cu	<50	19	18	18
W	<100	<25	<25	<25
H_2	<25	<5	<5	6
Hf	<100	45	35	36
Mg	<20	<10	<10	<10
Mn	<50	<25	<25	<25
Mo	<50	<25	<25	<25
N_2	<65	26	32	26
Nb	<100	<100	<100	<100
Ni	<70	<35	<35	<35
Pb	<130	<50	<50	<50
Si	<120	74	66	62

TABLE I (continued)

	Impurities (ppm) (continued)			
	Specification	Top	Middle	Bottom
Ta	<200	<200	<200	<200
Ti	<50	22	22	23
O_2	1000 to 1400	1030	1030	1040
U	<3.5	0.5	0.6	0.7
V	<50	<25	<25	<25

TABLE II

ZIRCALOY-4 CLADDING TUBING ANALYSIS PERFORMED BY TUBING MANUFACTURER (ppm)

	Specification	Sample 1	Sample 2
H_2	<25	9	11
N_2	<65	25	35
O_2	1000 to 1400	1120	1190

778 199

TABLE III

ZIRCALOY-4 CLADDING TUBING ANALYSIS PERFORMED BY FUEL ROD MANUFACTURER (ppm)

	Specification	Sample 1	Sample 2
H_2	<25	7.4	7.9
N_2	<65	49	36
O_2	1000 to 1400	1280	1261
Fe	--	21	20
Ni	<70	10	11

3. UNIAXIAL TENSILE PROPERTIES

The cladding tubing was specified to be cold worked a minimum of 50%, and stress-relieved, and to have the following minimum room temperature longitudinal tensile properties: yield strength (0.2% offset), 413.64 MPa; ultimate tensile strength, 482.58 MPa; total elongation (in 50 mm), 16%.

The zircaloy-4 tubing mechanical properties were characterized by uniaxial tensile tests conducted by the tubing manufacturer at temperatures ranging from room temperature to 1255 K. The yield strength, ultimate tensile strength, and total elongation are listed in Table IV, and plotted versus temperature in Figures 4, 5, and 6, respectively. Ingot and tubing hardness analysis results provided by the tubing manufacturer are also presented in Table IV.

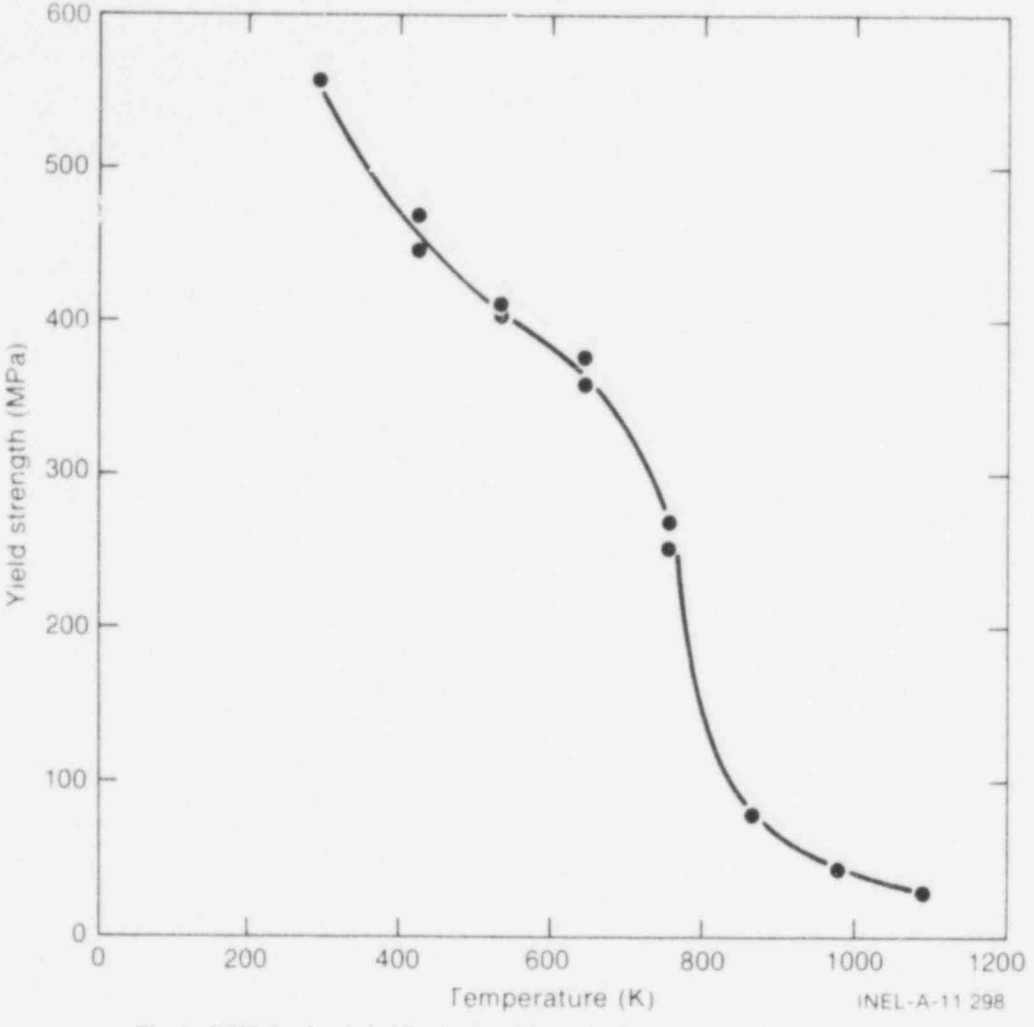

Fig. 4 PCM zircaloy-4 cladding tubing yield strength as a function of temperature.

778 201

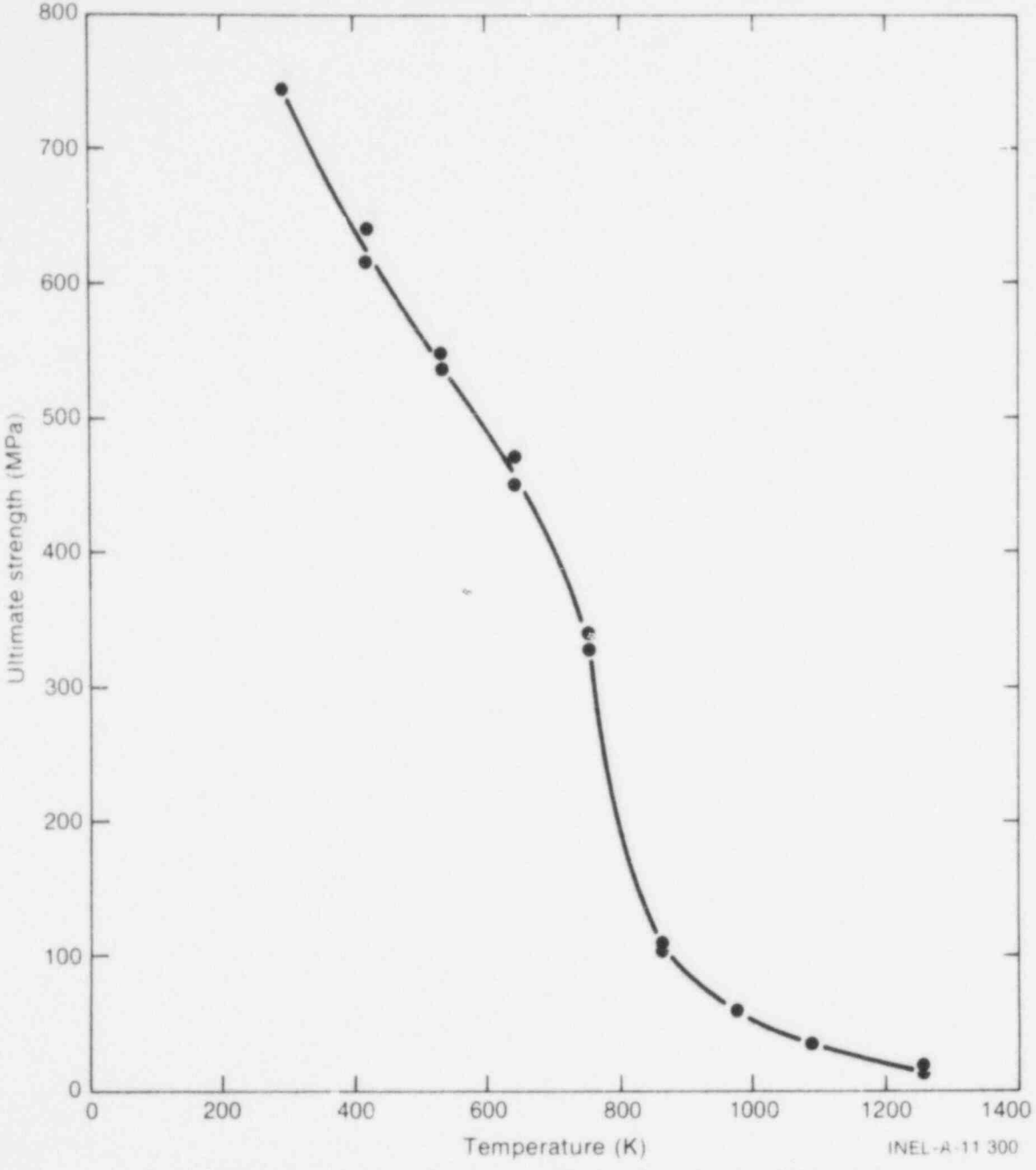

Fig. 5 PCM zircaloy-4 cladding tubing ultimate tensile strength as a function of temperature.

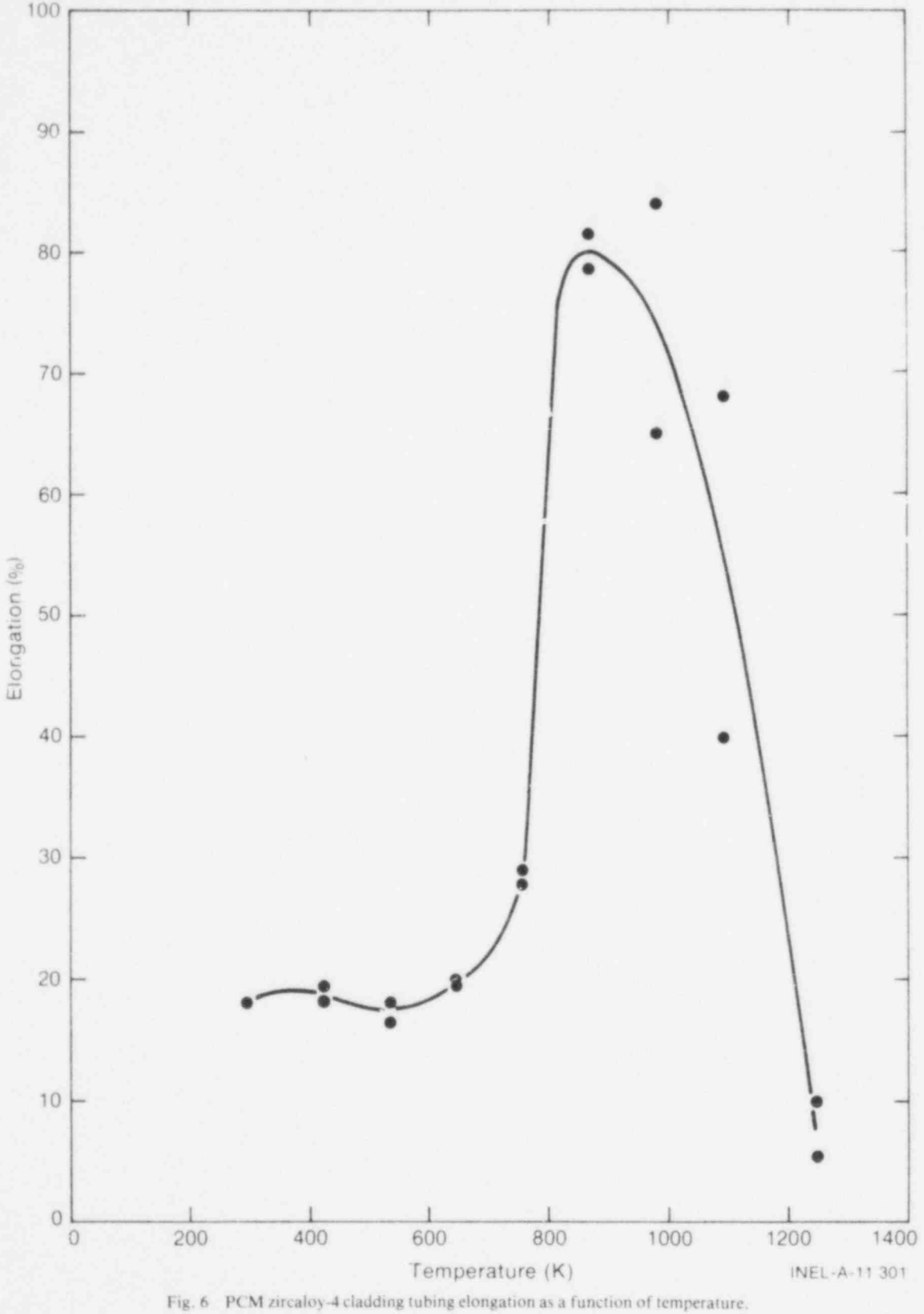

Fig. 6 PCM zircaloy-4 cladding tubing elongation as a function of temperature.

778 203

TABLE IV

ZIRCALOY-4 CLADDING TUBING MECHANICAL PROPERTIES DETERMINED BY TUBING MANUFACTURER

Temperature (K)	Yield Strength (MPa)	Ultimate Tensile Strength (MPa)	Elongation (%)
Room	558	745	18
Room	558	745	18
422	447	614	19.5
422	467	641	18
533	404	537	18
533	410	547	16.5
644	357	452	19.5
644	376	471	20
755	269	341	29
755	252	327	28
866	80	111	81.5
866	78	103	78.5
977	44	61	65
977	44	61	84
1089	28	35	40
1089	28	35	68
1255	[a]	18	10
1255	[a]	14	5.5

[a] Extensometer broke.

778 204

TABLE IV (continued)

Ingot Hardness Analysis (BHN)		
	Specification	Results
Range	187 maximum	163 to 181
Average	170 to 183	174

Tubing Hardness Analysis	
Distance from Outside Diameter Surface (mm)	DPH Measurements
0.025	195
0.127	208
0.227	215
0.330	208
0.431	205

4. BURST CHARACTERISTICS

PCM cladding bursting was characterized by out-of-reactor burst tests of unirradiated cladding to provide reference data on burst temperature, pressure, and circumferential strain for comparison with in-reactor PCM Test Series cladding bursting. The burst tests were conducted by the Material Science Division at the Argonne National Laboratory (ANL) in Argonne, Illinois, and the results compared with NRC standard cladding burst test results. The dimensions of the NRC standard cladding (10.92-mm outside diameter, 9.65-mm inside diameter, 0.635-mm wall thickness) are slightly different from the PCM cladding dimensions (10.72-mm outside diameter, 9.50-mm inside diameter, 0.61-mm wall thickness); however, the textures of both lots of material are similar and the results compare well.

The test pieces of PCM cladding contained Al_2O_3 simulated fuel pellets as internal constraints, machined to give a 0.075-mm diametral pellet-to-cladding gap. The ten cladding samples were initially pressurized with argon to different pressures, and heated to bursting in a steam environment. The initial pressures ranged from 1.0 to 9.4 MPa which resulted in bursts at temperatures in the α-, ($\alpha + \beta$)-, and β-phase regions. The heating rates for all samples except one ranged from 34 to 62 K/s, which are representative of the heating rates the PCM cladding experiences in the Power Burst Facility reactor. The cladding sample initial pressures and burst test results are given in Table V.

PCM cladding maximum circumferential strain and results of NRC standard cladding tests performed at several heating rates are plotted versus cladding sample initial pressure in Figure 7. In-reactor burst data from the KfK FR-2 reactor experiments are also shown. The PCM cladding burst test results obtained for heating rates of 34 to 62 K/s, Samples PBF-1 and PBF-3 through -10, are in good agreement with the NRC standard cladding burst test results obtained for a heating rate of ~45 K/s. The PCM cladding results

TABLE V

CLADDING BURST TEST SAMPLE INITIAL PRESSURES AND RESULTS

Cladding Sample	Initial Pressure at 300 K (MPa)	Heating Rate[a] (K/s)	Maximum Recorded Burst Temperature (K)	Maximum Circumferential Burst Strain
PBF-1	6.73	43	1035	0.19
PBF-2	9.41	8	1029	0.69
PBF-3	2.71	48	1142	0.20
PBF-4	6.73	∿50[b]	951	0.20
PBF-5	2.71	∿50[b]	1134	0.21
PBF-6	9.41	42	1078	0.29
PBF-7	9.41	53	928	0.23
PBF-8	6.73	34	1046	0.21
PBF-9	1.00	43	1340	0.34
PBF-10	9.48	62	1031	0.25

[a] Heating rate was determined from the thermocouple nearest the burst region over the temperature range of 650 to 1080 K.

[b] Estimated value.

obtained for a heating rate of 8 K/s, Sample PBF-2, are also in good agreement with the corresponding NRC standard cladding results.

PCM cladding recorded burst temperature and results of NRC standard cladding tests performed at several heating rates are plotted versus cladding sample initial pressure in Figure 8. In-reactor burst data from the KfK FR-2 reactor experiments are also shown. The PCM cladding and NRC standard cladding results compare well, although there is some indication that the thinner-walled PCM cladding bursts at a slightly lower temperature.

The ten PCM cladding burst test samples with cross sections of each sample at the region of maximum circumferential strain are shown after bursting in Figures 9 through 18.

The high pressure, high heating rate (9.4 MPa, 42 to 62 K/s) samples, Samples PBF-6, -7 and, -10 (Figures 14, 15, and 18, respectively), show rupture-type failures[2], that is, sharp fracture edges as a result of considerable localized cladding wall thinning. The burst temperature, burst pressure, and metallography of these samples in the fracture areas indicate the cladding temperature was in the α- or predominately α-phase region at burst. Similar observations have been made for the NRC standard cladding in a steam environment, at high heating rates (> 70 K/s) and with tightly constrained cladding. This

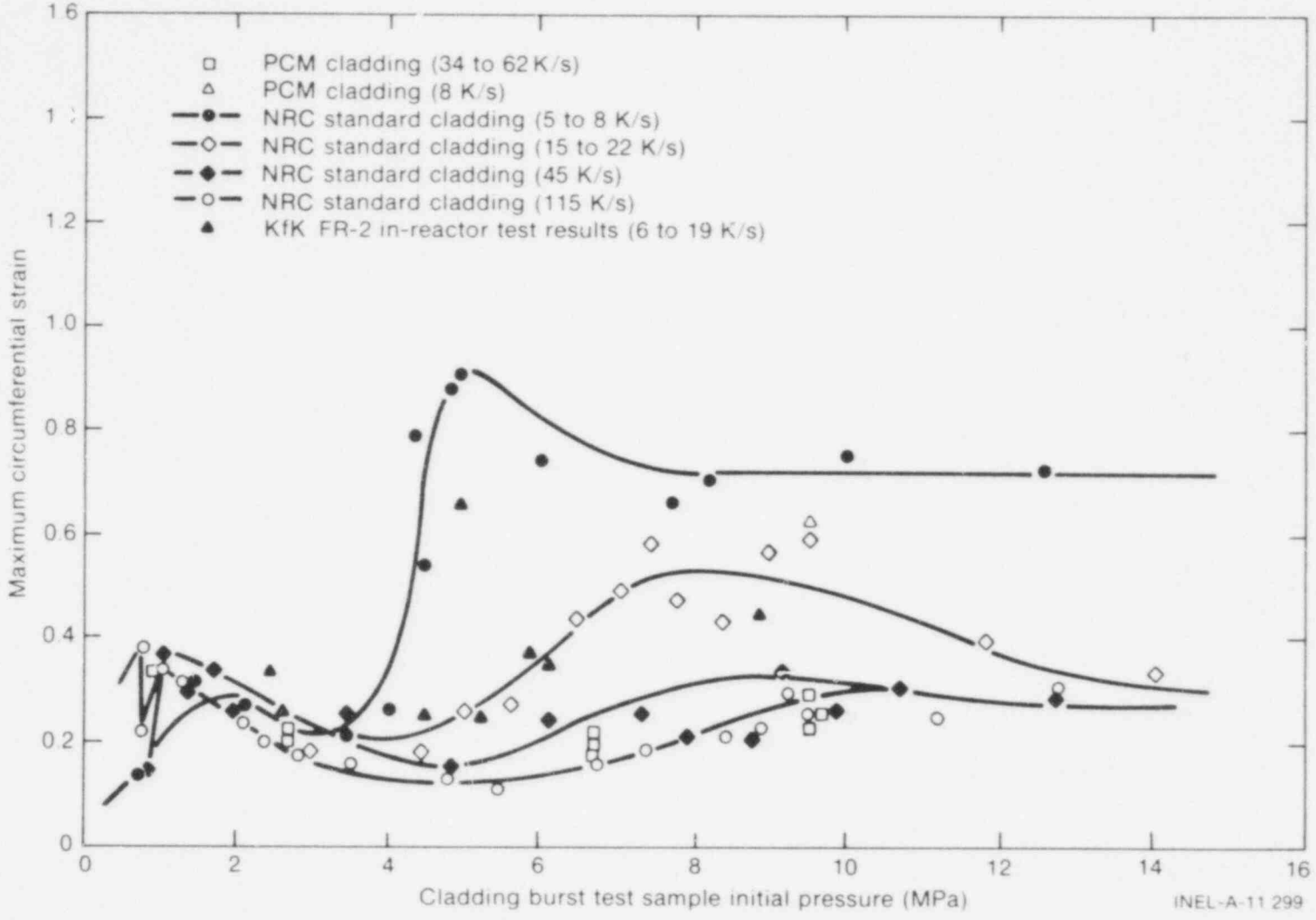

Fig. 7. Maximum circumferential strain versus cladding burst test sample initial pressure for PCM and NRC standard cladding.

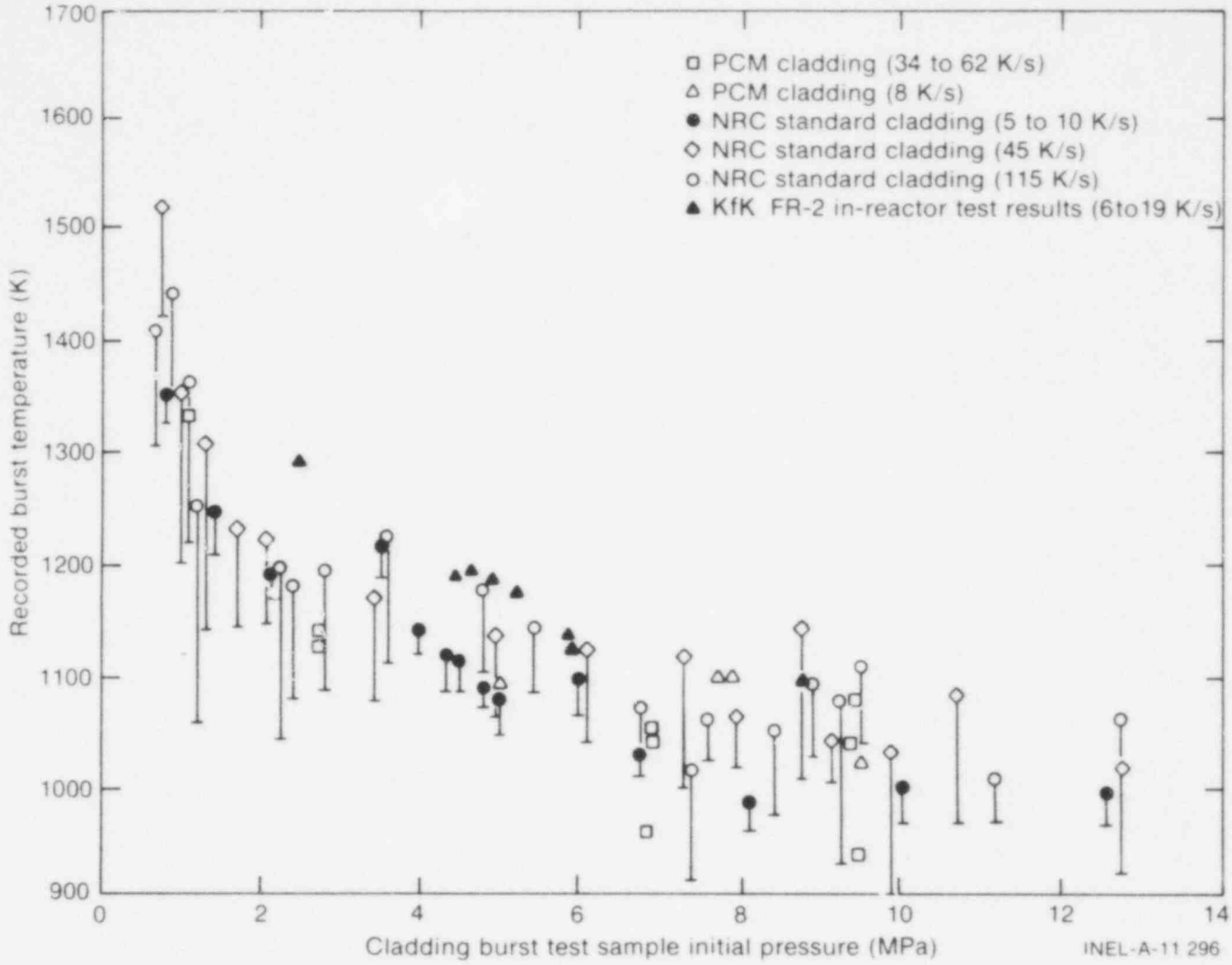

Fig. 8 Recorded burst temperature versus cladding burst test sample initial pressure for PCM and NRC standerd cladding.

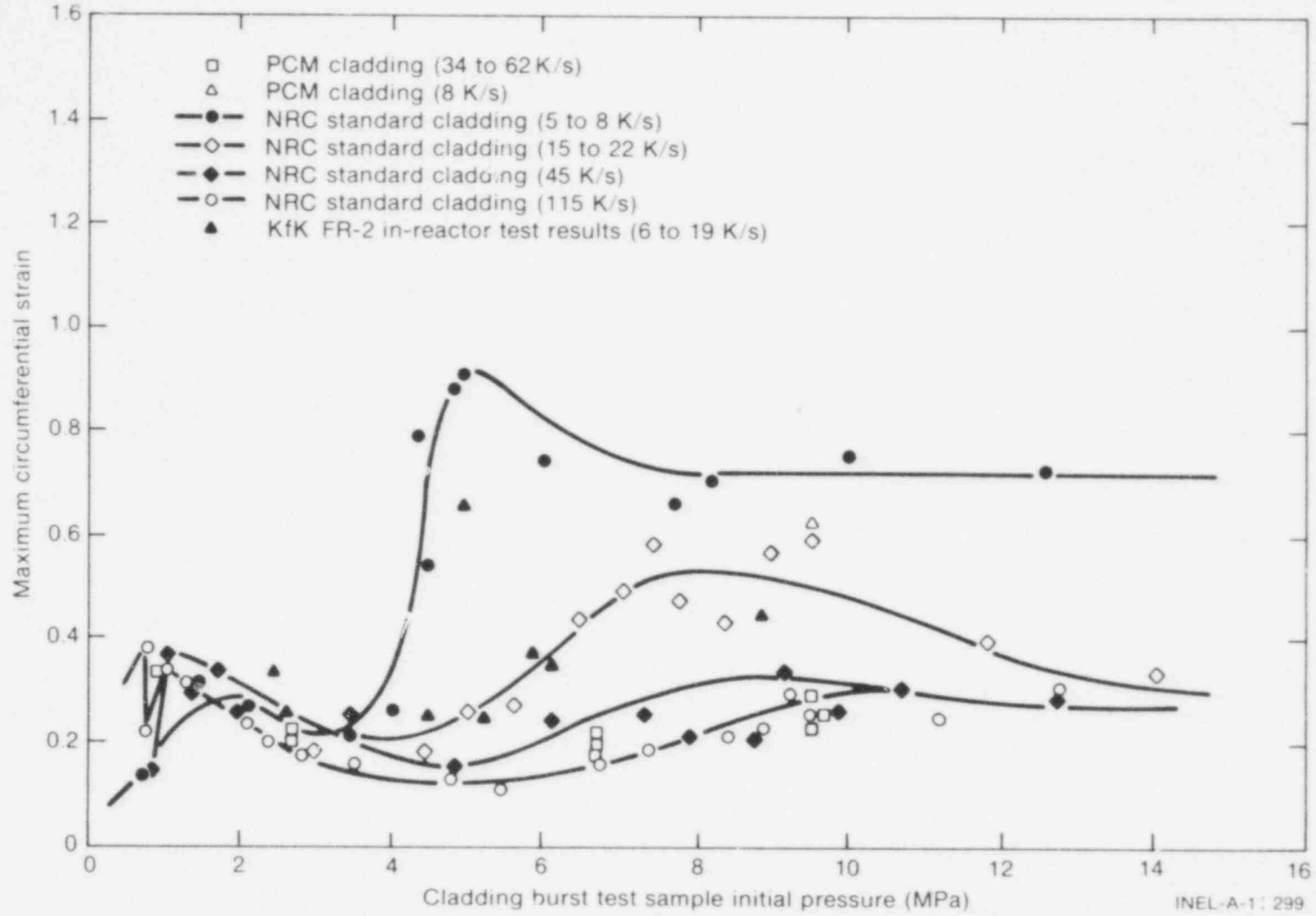

Fig. 7 Maximum circumferential strain versus cladding burst test sample initial pressure for PCM and NRC standard cladding.

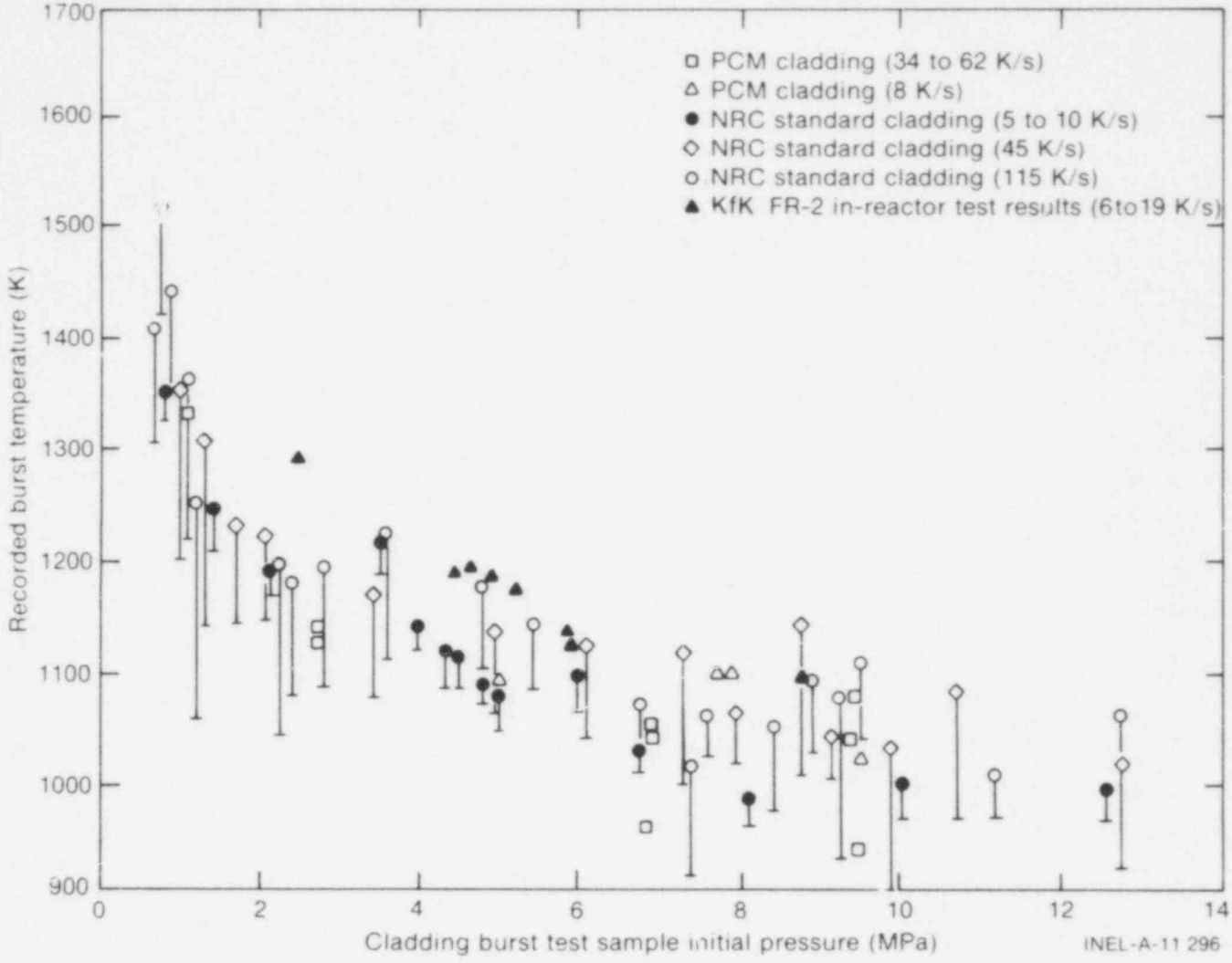

Fig. 8 Recorded burst temperature versus cladding burst test sample initial pressure for PCM and NRC standard cladding.

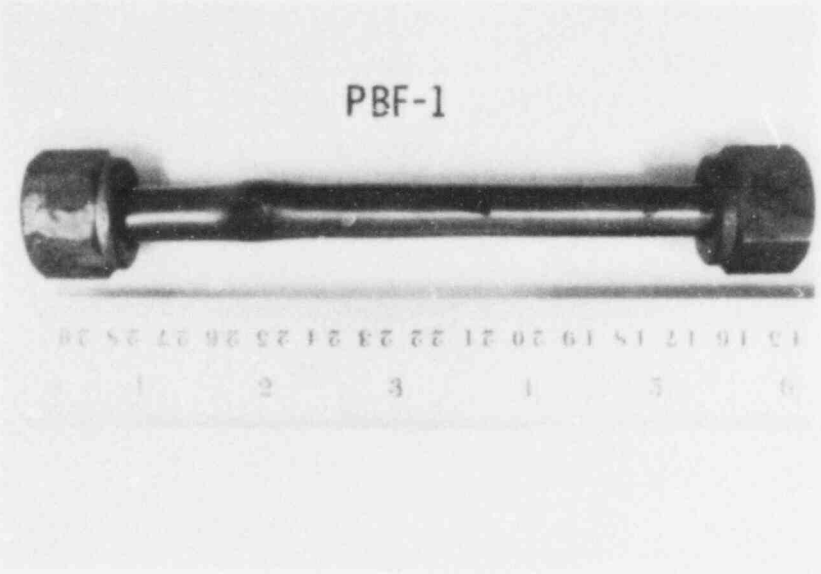

a. Cladding sample after burst

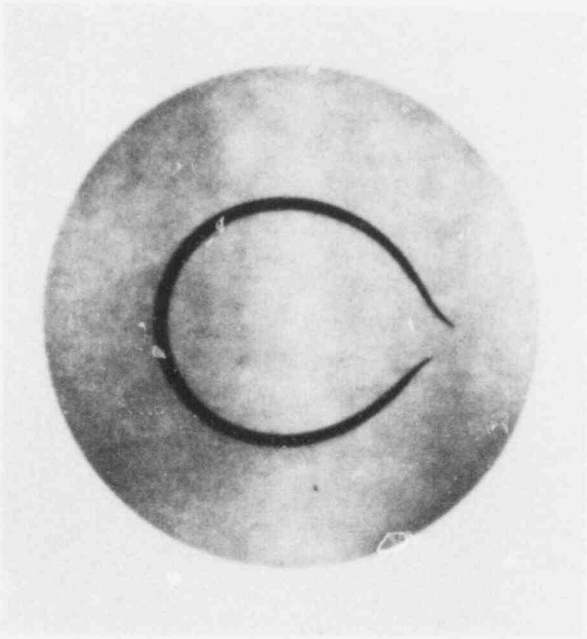

b. Cross section in the region of maximum circumferential strain

GS-008-20

Fig. 9 Cladding Sample PBF-1 after burst in steam (heating rate 43 K/s, initial pressure 6.73 MPa).

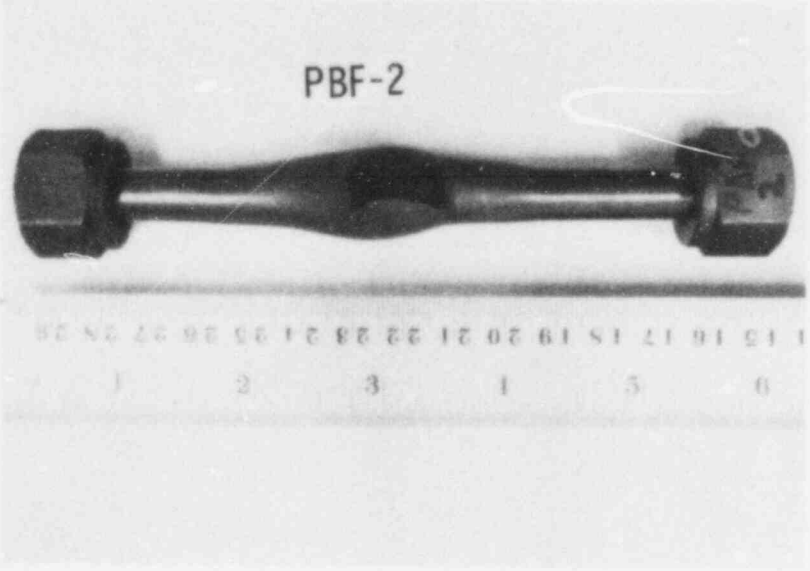

a. Cladding sample after burst

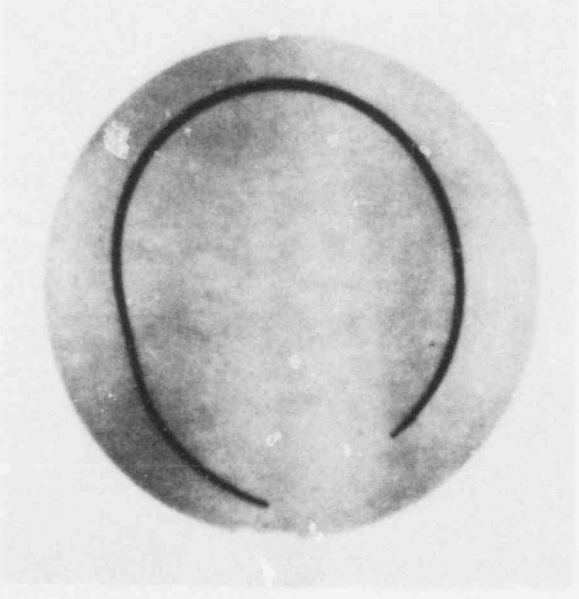

b. Cross section in the region of maximum circumferential strain

GS-008-21

Fig. 10 Cladding Sample PBF-2 after burst in steam (heating rate 8 K/s, initial pressure 9.41 MPa).

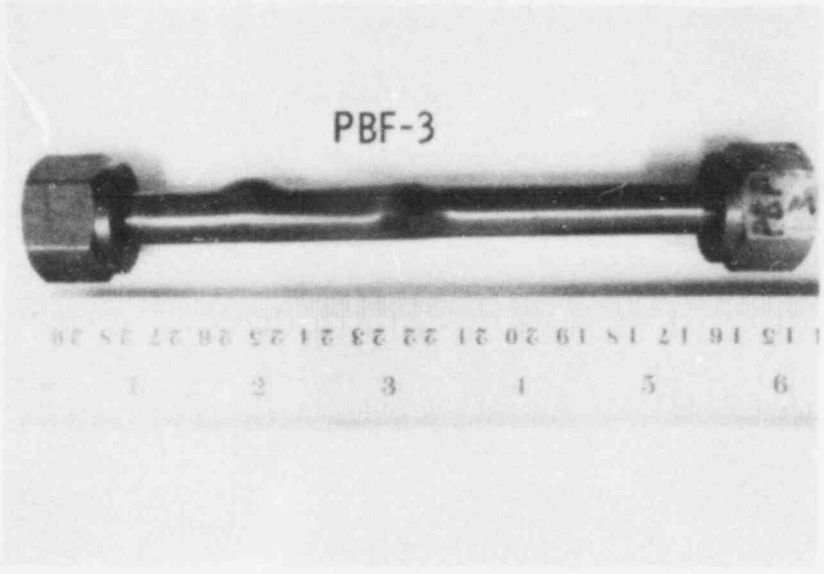

a. Cladding sample after burst

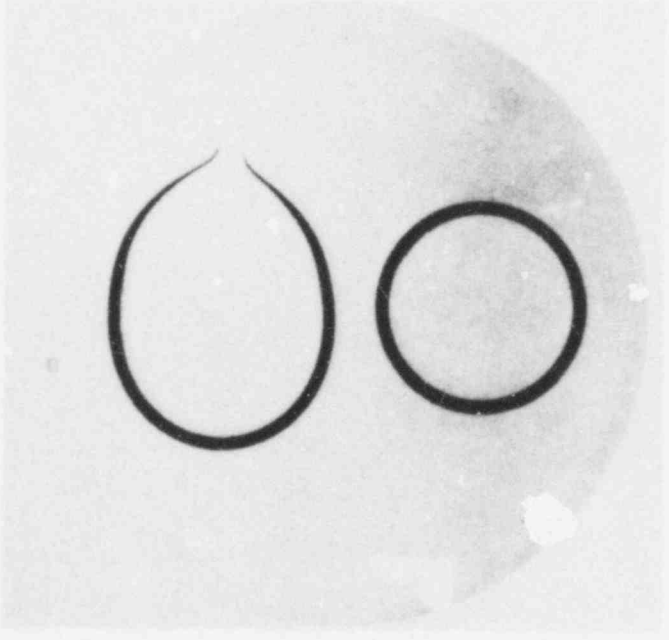

b. Cross section of original cladding and the region of maximum circumferential strain

GS-008-22

Fig. 11 Cladding Sample PBF-3 after burst in steam (heating rate 48 K/s, initial pressure 2.71 MPa).

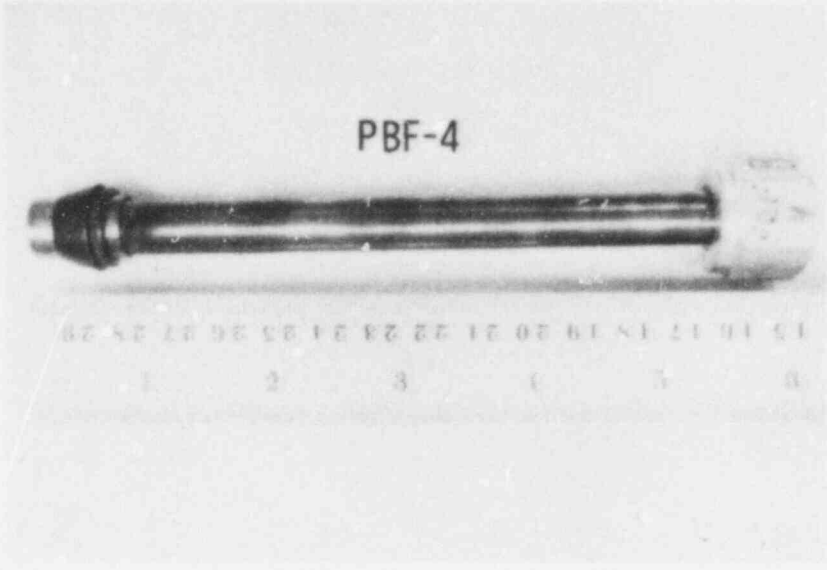

a. Cladding sample after burst

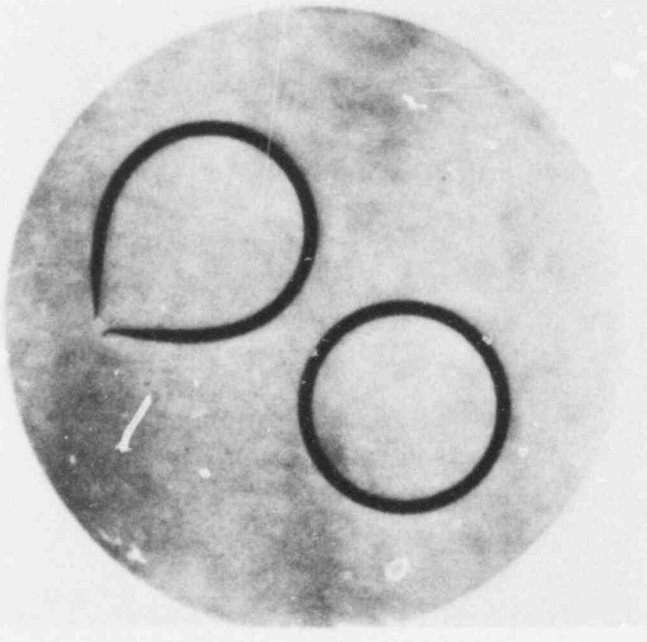

b. Cross section of original cladding and the region of maximum circumferential strain

GS-008-23

Fig. 12 Cladding Sample PBF-4 after burst in steam (heating rate 50 K/s, initial pressure 6.73 MPa).

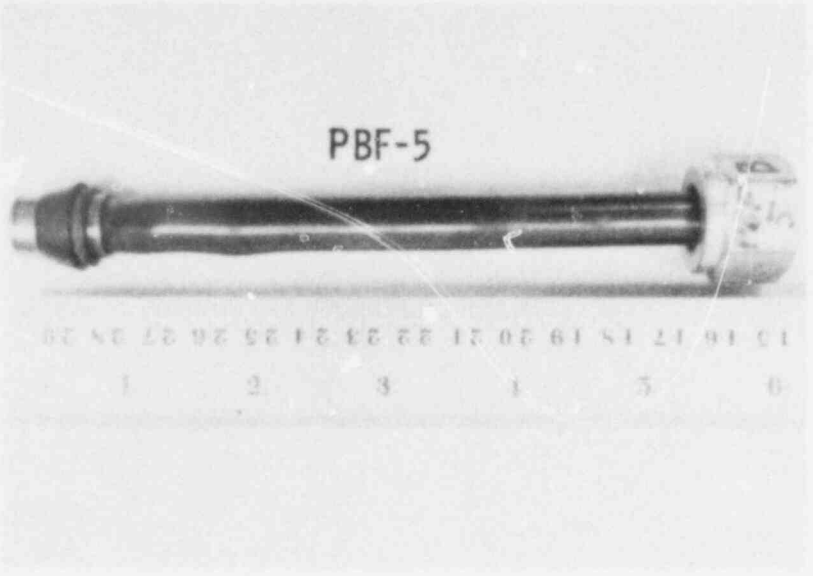

a. Cladding sample after burst

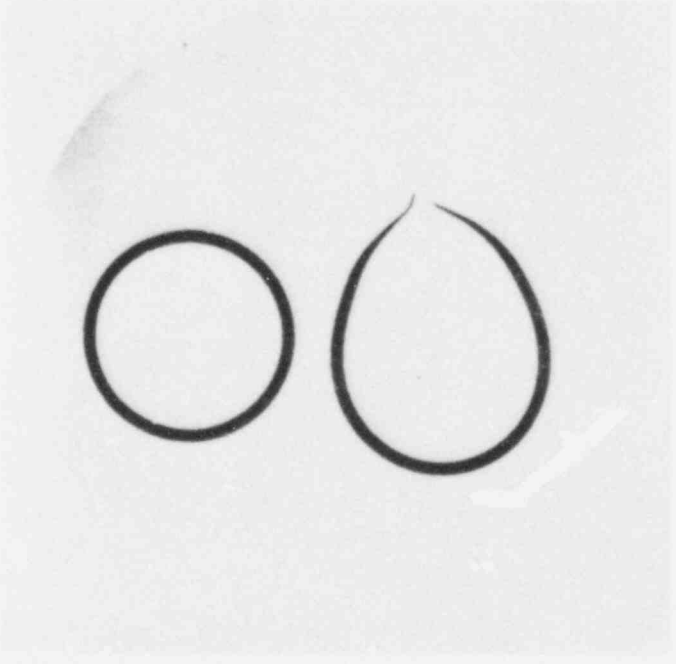

b. Cross section of original cladding and the region of maximum circumferential strain

GS-008-24

Fig. 13 Cladding Sample PBF-5 after burst in steam (heating rate 50 K/s, initial pressure 2.71 MPa).

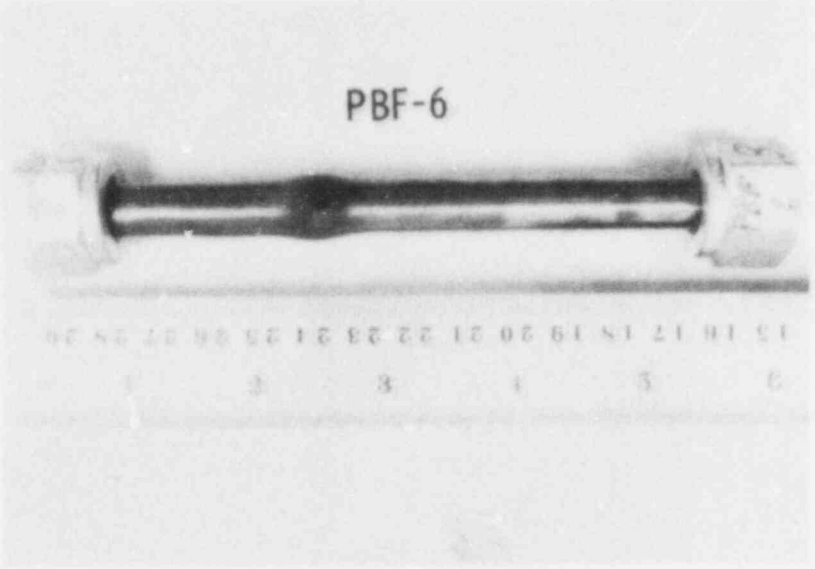

a. Cladding sample after burst

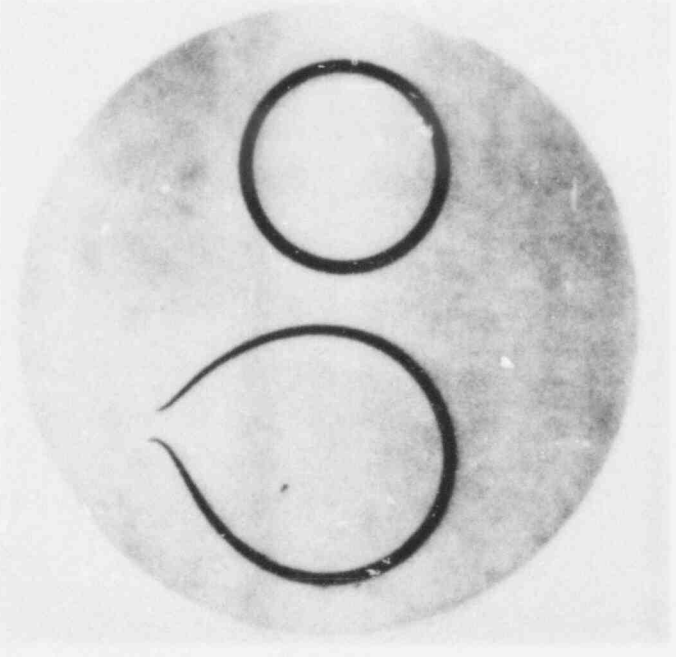

b. Cross section of original cladding and the region of maximum circumferential strain

GS-008-25

Fig. 14 Cladding Sample PBF-6 after burst in steam (heating rate 42 K/s, initial pressure 9.41 MPa).

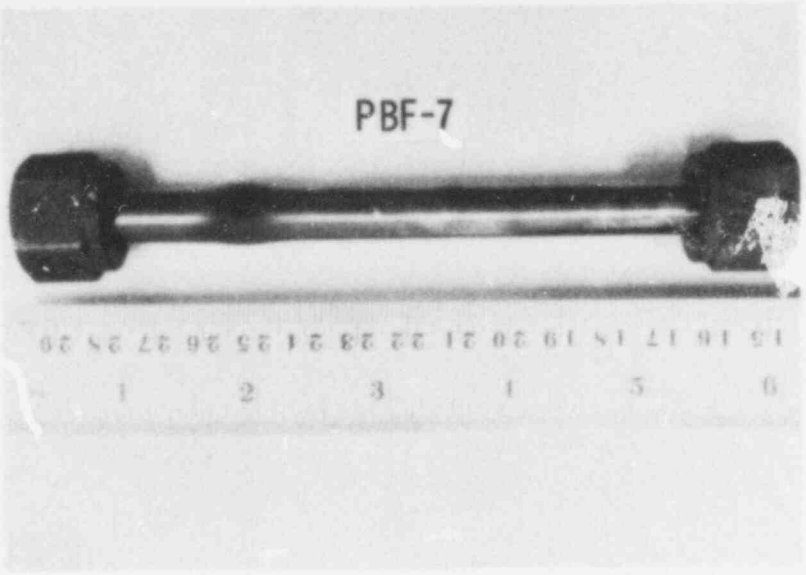

a. Cladding sample after burst

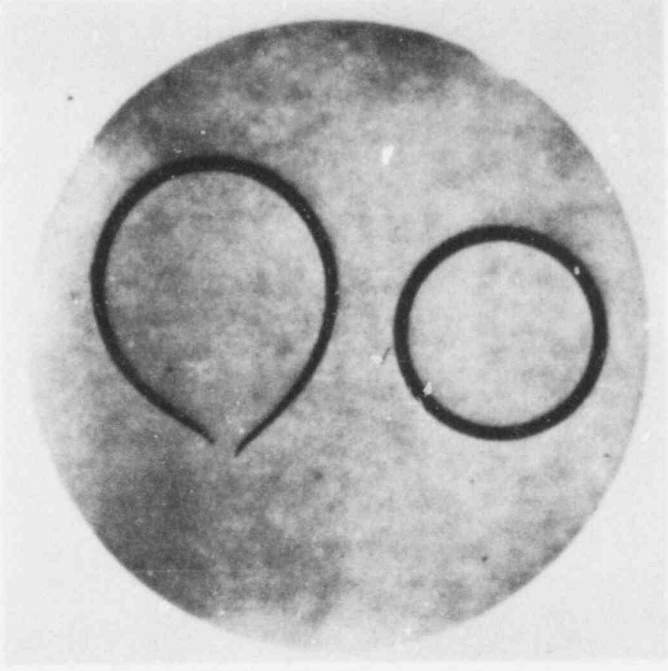

b. Cross section of original cladding and the region of maximum circumferential strain

GS-008-26

Fig. 15 Cladding Sample PBF-7 after burst in steam (heating rate 53 K/s, initial pressure 9.41 MPa).

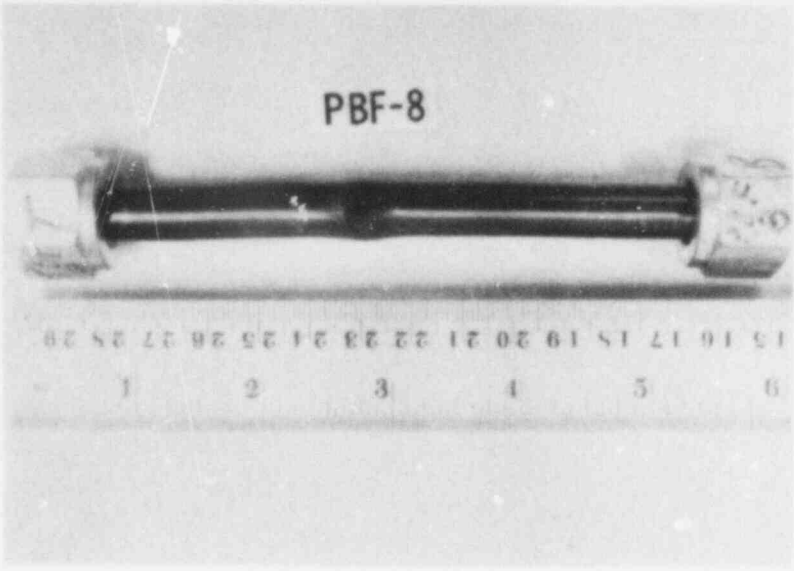

a. Cladding sample after burst

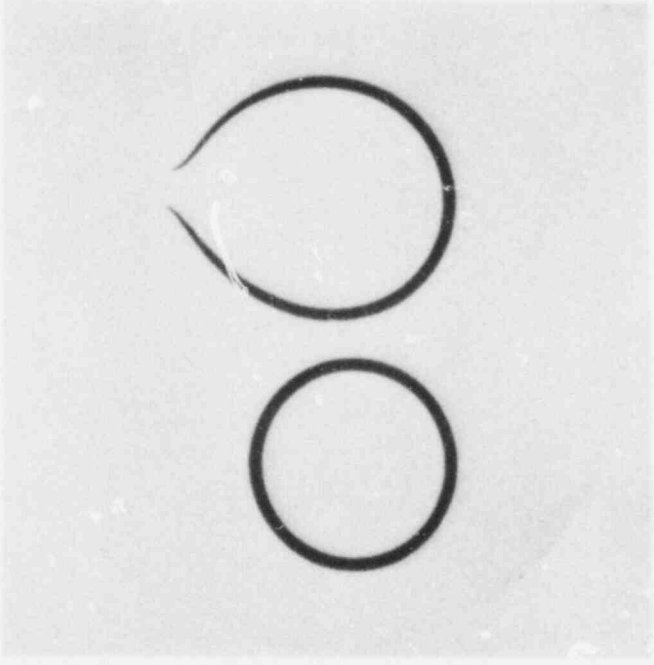

b. Cross section of original cladding and the region of maximum circumferential strain

GS-008-27

Fig. 16 Cladding Sample PBF-8 after burst in steam (heating rate 34 K/s, initial pressure 6.73 MPa).

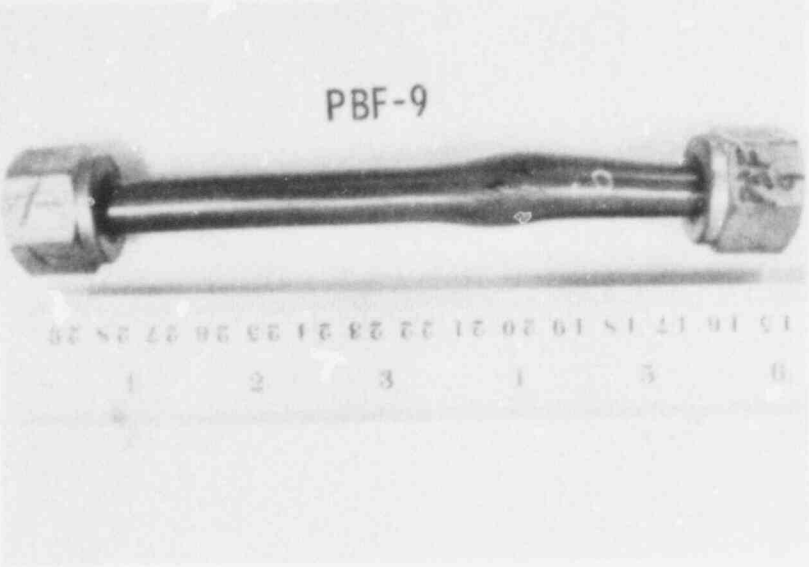

a. Cladding sample after burst

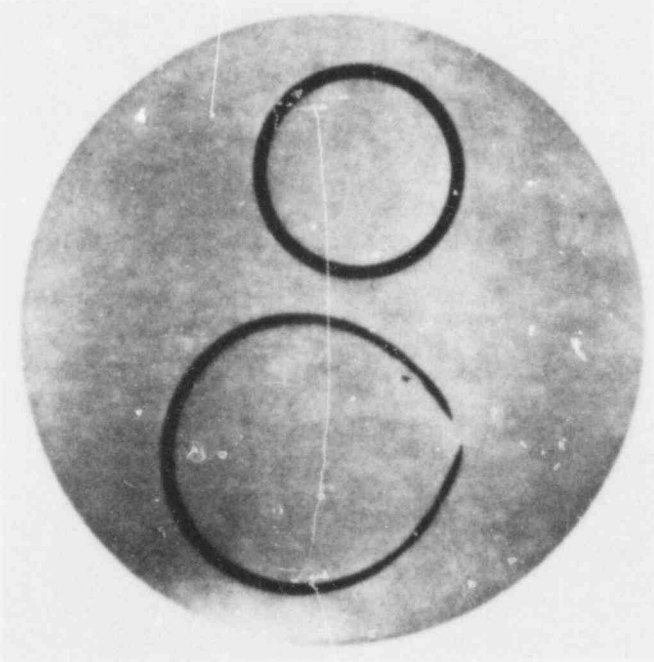

b. Cross section of original cladding and the region of maximum circumferential strain

GS-008-28

Fig. 17 Cladding Sample PBF-9 after burst in steam (heating rate 43 K/s, initial pressure 1.0 MPa).

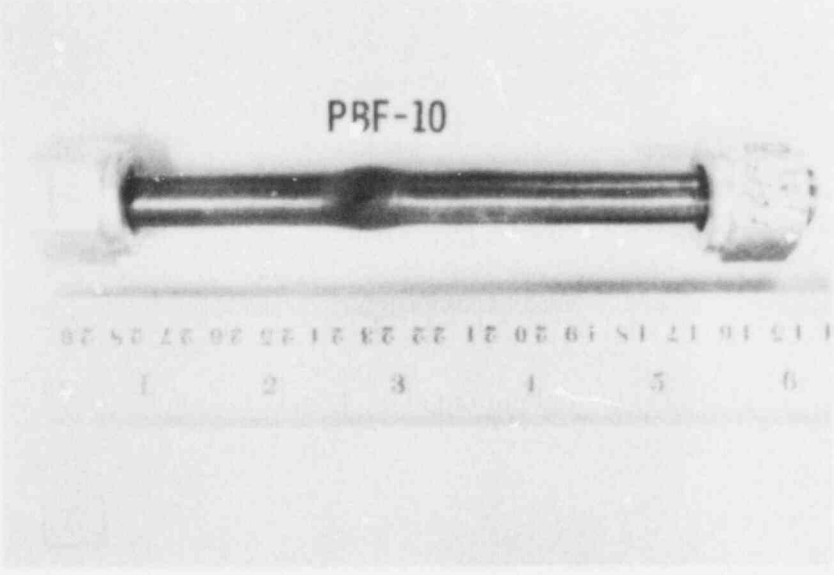

a. Cladding sample after burst

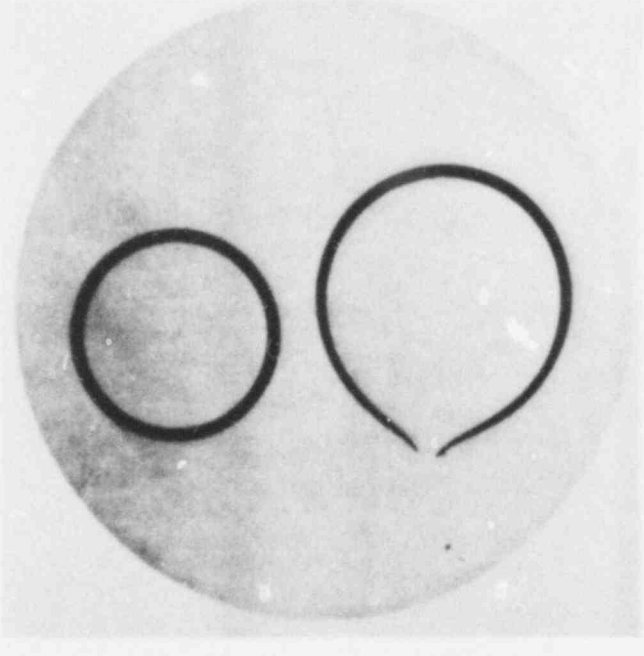

b. Cross section of original cladding and the region of maximum circumferential strain

GS-008-29

Fig. 18 Cladding Sample PBF-10 after burst in steam (heating rate 62 K/s, initial pressure 9.48 MPa).

observed rupture-type failure of α-phase cladding indicates one of the following three deformation processes: (a) pyramidal slip with $(\vec{a} + \vec{c})$-type Burgers vector, (b) $\{11\bar{2}2\}$ twinning, and (c) grain rotation in which texture is destroyed during deformation. Apparently, a high strain rate and severe constraint against axial contraction and tube bending are prerequisites for the rupture-type failure of α-phase cladding.

The high pressure, low heating rate (9.4 MPa, 8 K/s) sample, Sample PBF-2 (Figure 10), shows a fracture-type failure[2] of α-phase material, that is, a shear fracture with blunt fracture edges. The fracture-type failure tip indicates cladding resistance against wall thinning and, hence, large circumferential cladding expansion. Similar observations have been made for the NRC standard cladding in a steam environment at low heating rates (< 30 K/s).

Previously reported ANL test results support the PCM cladding burst test observations[2,3]. Rupture-type bursts in the α-phase region during transient-heating experiments result from temperature nonuniformities in the cladding (at heating rates of ~45 K/s), which decrease the circumferential strain at failure. At low heating rates (8 K/s for PCM cladding and <30 K/s for NRC standard cladding) and high initial pressures (>7 MPa), the cladding temperatures were circumferentially uniform, increasing the circumferential strain at failure and resulting in large circumferential cladding expansion. At lower internal pressures, the cladding typically ruptured at temperatures in the ($\alpha + \beta$) two-phase or β-phase regions, and zircaloy oxidation rather than temperature nonuniformity limited the circumferential strain at failure.

The lower pressure (6.73 MPa) samples, Samples PBF-1, -4, and -8 (Figures 9, 12, and 16, respectively), show rupture-type failures of α-phase material typical of approximately 7 MPa initial pressure. The lower pressure (2.71 MPa) samples, Samples PBF-3 and -5 (Figures 11 and 13, respectively), show rupture-type failures typical of ($\alpha + \beta$) two-phase material. The lowest pressure (1.00 MPa) sample, Sample PBF-9 (Figure 17), shows a fracture-type failure typical of brittle β-phase material.

5. MICROSTRUCTURE

A transverse section and a longitudinal section of PCM zircaloy-4 cladding were examined metallographically at EG&G Idaho, Inc. Figures 19 and 20 show the observed microstructure of the transverse and longitudinal sections, respectively, at 100x and 400x magnification. The average grain size as reported by Gulf United Nuclear Fuels Corporation is ASTM grain size 11.8, which is equivalent to 6 μm.

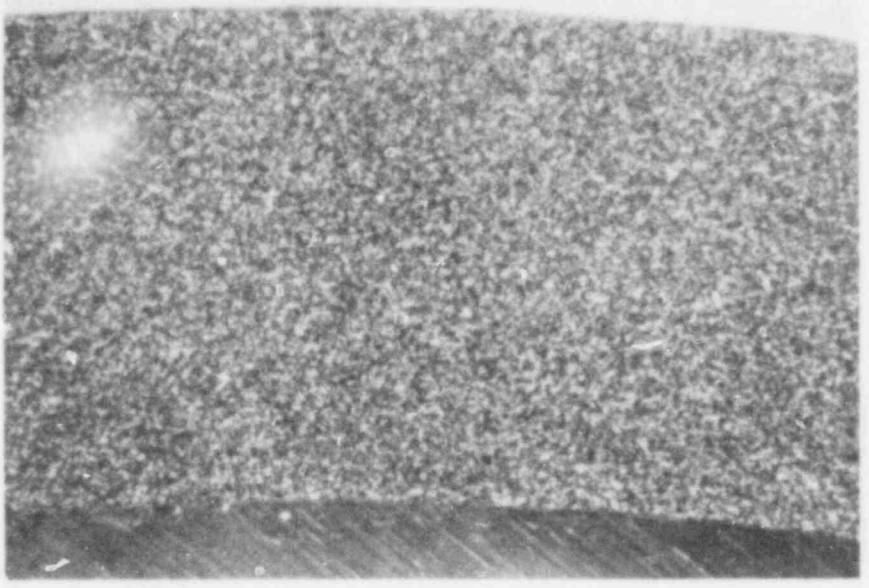

Etched, polarized light (a) 100 μm

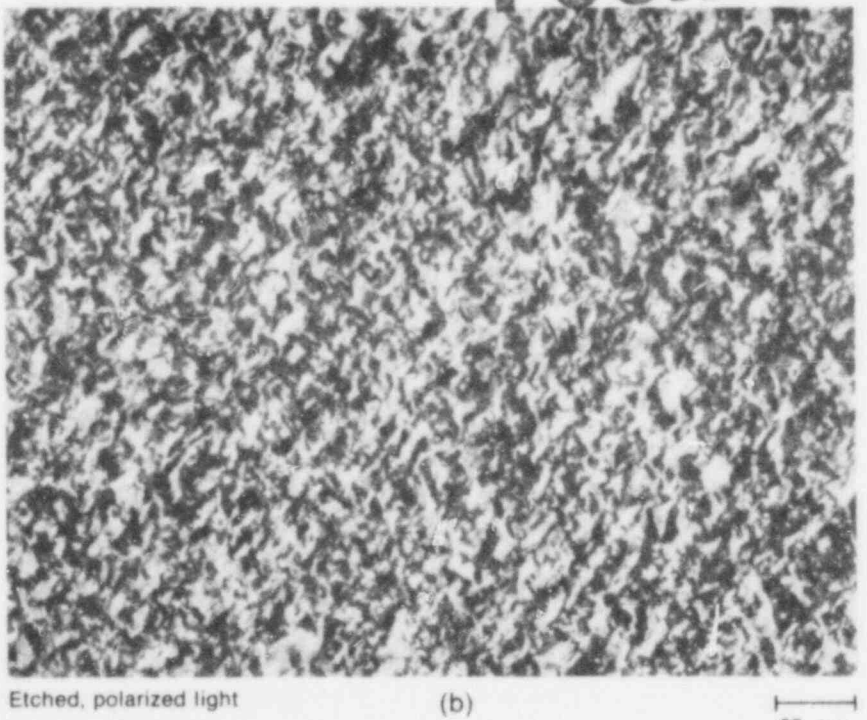

Etched, polarized light (b) 25 μm

GS-008-1

Fig. 19 PCM cladding microstructure (transverse section).

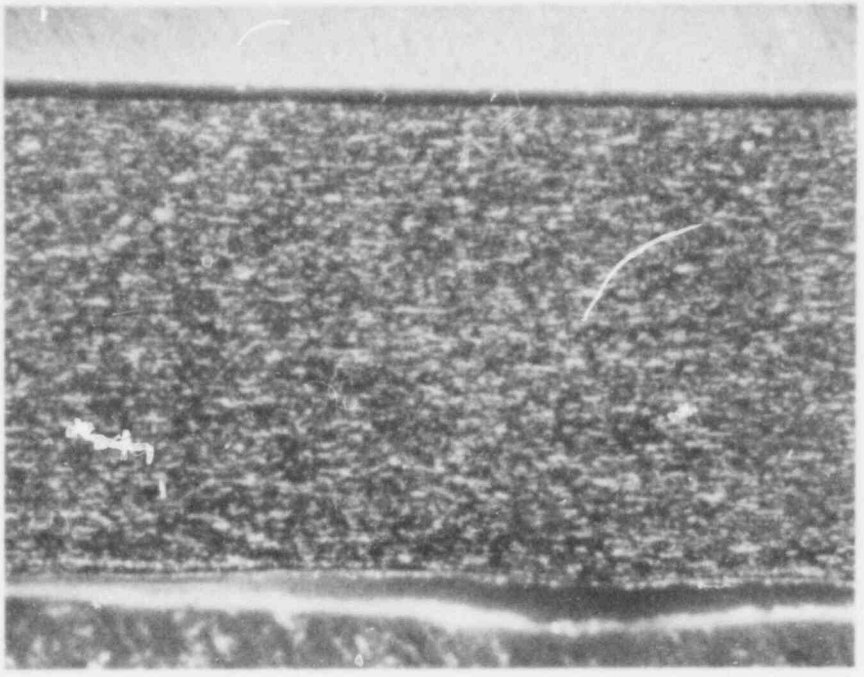

Etched, polarized light (a) 100 μm

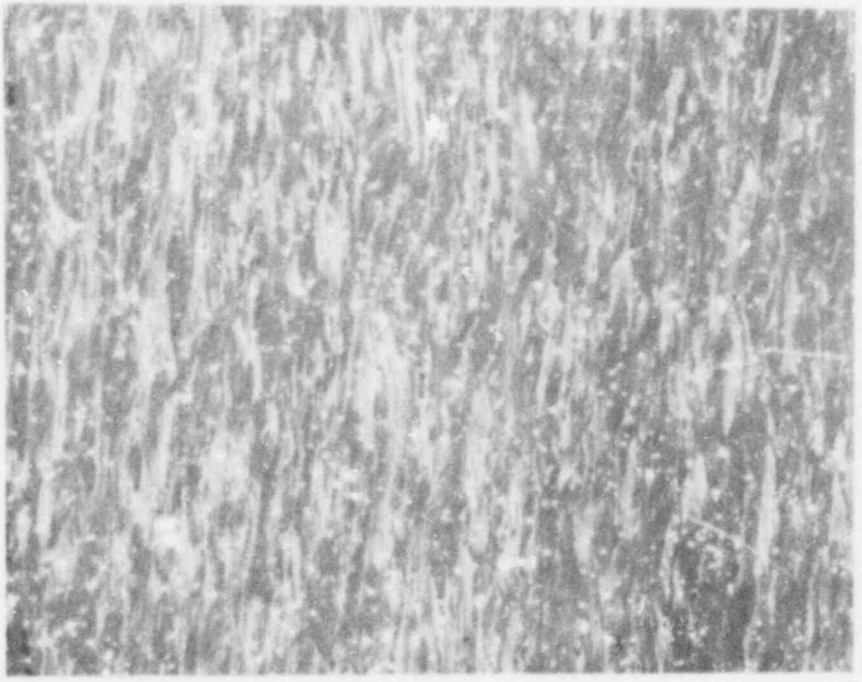

Etched, polarized light (b) 25 μm

GS-008-2

Fig. 20 PCM cladding microstructure (longitudinal section).

6. CRYSTALLOGRAPHIC TEXTURE

The crystallographic texture of PCM cladding tubing was determined by X-ray diffraction measurements of three mutually perpendicular tubing surfaces (tangential, axial, and radial). The ratio of observed diffraction intensity from a particular crystal plane to the expected intensity of a similar surface with random crystal plane orientations is expressed as a texture coefficient[4]. A texture coefficient of 1 indicates that the orientation of crystal planes in that sample is random. A texture coefficient greater than 1 indicates that the sample has more planes oriented in the crystallographic direction examined than a random sample, and a texture coefficient less than 1 indicates that the sample has fewer planes oriented in the direction examined than the random sample.

In Figures 21, 22, and 23, the texture coefficients for the PCM tubing are plotted for the tangential, axial, and radial directions, respectively, using the inverse pole figure technique. In this technique, the texture coefficients are plotted on a stereographic projection of the lattice and contour lines are drawn to indicate preferred orientations of the crystal planes, for each of the three mutually perpendicular surfaces examined. The texture coefficients for the three directions examined are tabulated in Table VI. The (0002) basal poles lie in both the tangential and radial directions with about 56% of the poles in the tangential direction. The texture coefficient of the $(10\bar{1}0)$ poles in the axial direction (5.02) is about twice the texture coefficient of the basal poles in either the tangential or radial directions (normally this ratio is about one), indicating that each of the basal pole orientations could be contributing to the $(10\bar{1}0)$ axial orientation. The ratio of the $(10\bar{1}0)$ to the $(11\bar{2}0)$ texture coefficients in the axial direction has been used by Berman et al.[4] as a measure of the amount of cold deformation. This ratio of 6.52 indicates extensive residual cold work in the cladding.

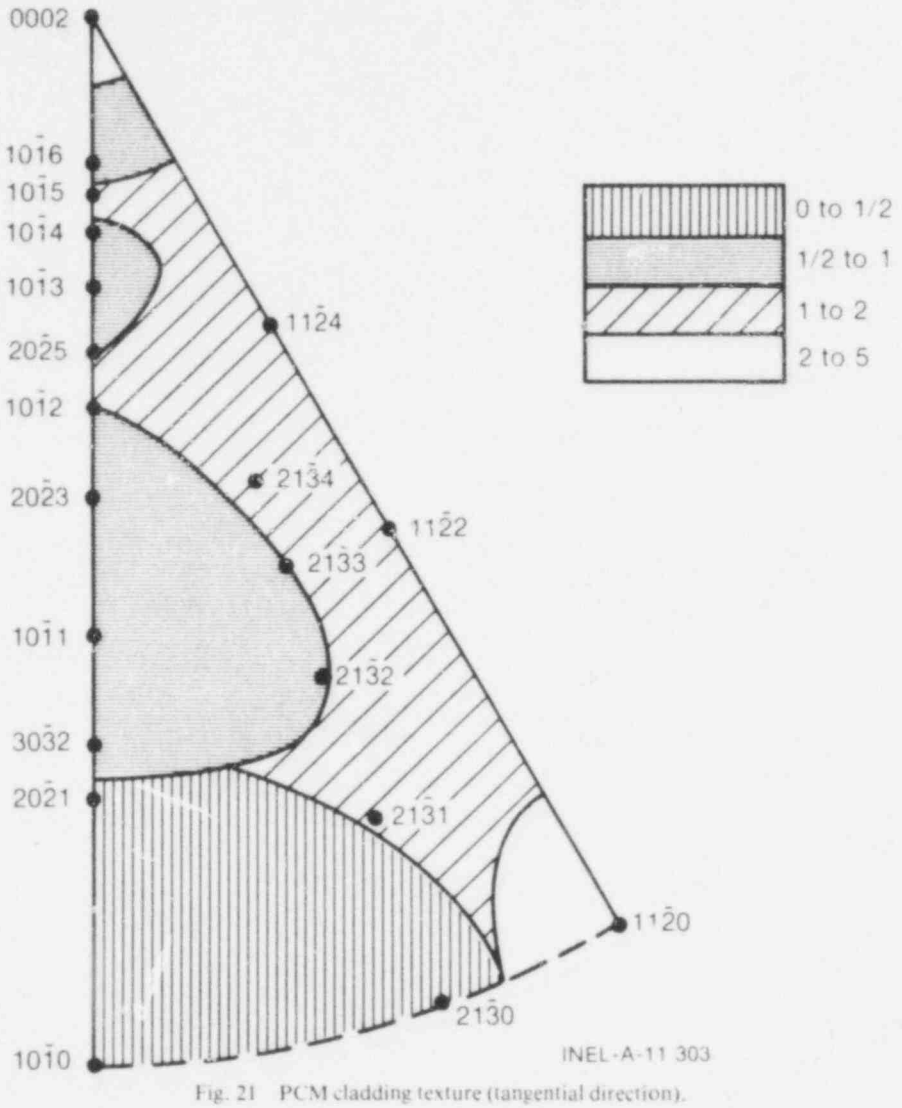

Fig. 21 PCM cladding texture (tangential direction).

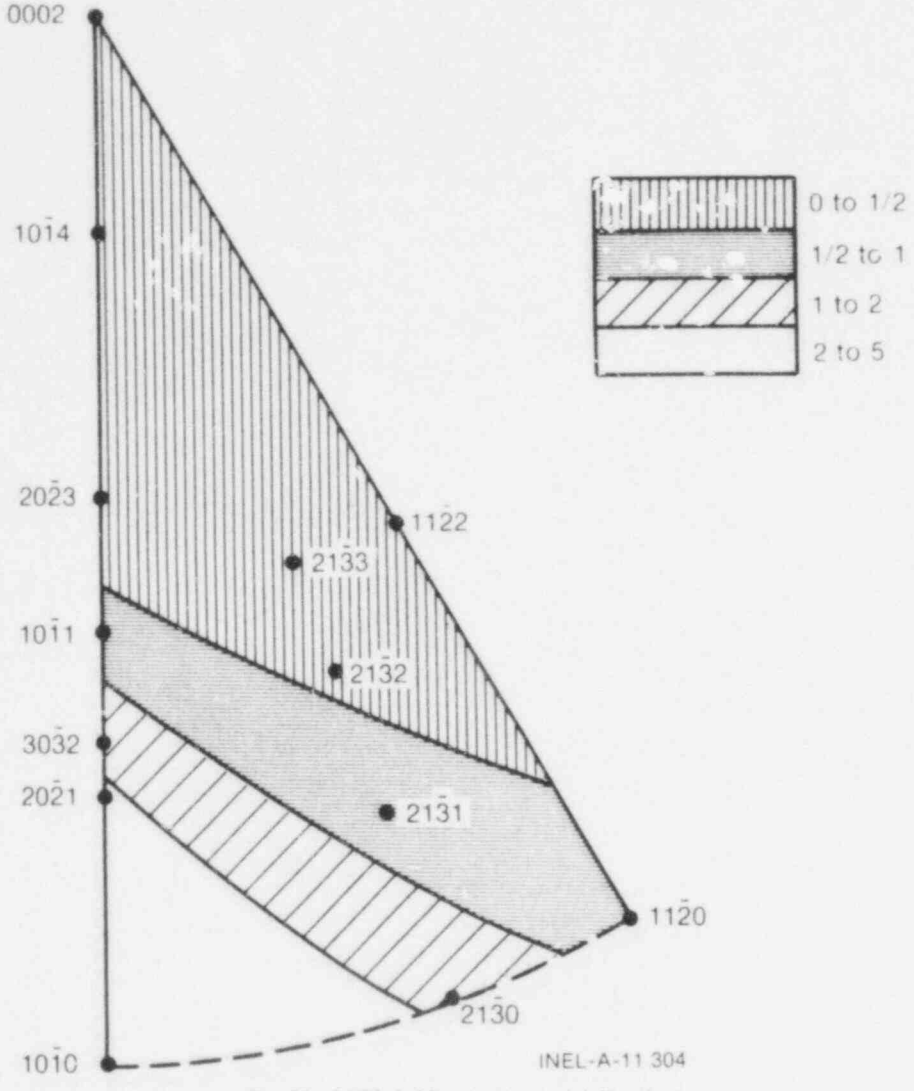

Fig. 22 PCM cladding texture (axial direction).

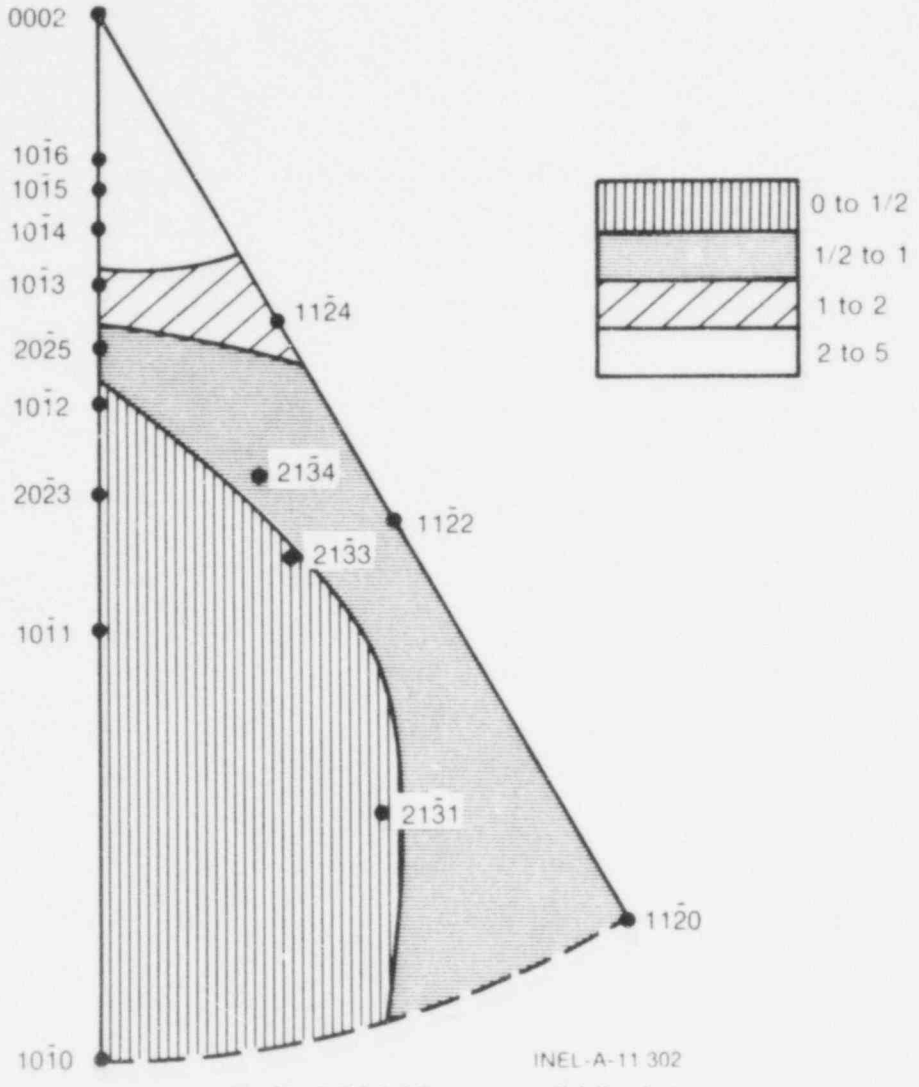

Fig. 23 PCM cladding texture (radial direction).

TABLE VI

CLADDING INVERSE POLE FIGURE TECHNIQUE TEXTURE COEFFICIENTS

	Texture Coefficients		
Crystal Plane	Tangential	Axial	Radial
$10\bar{1}0$	0.36	5.02	0.05
0002	2.63	0.09	2.10
$10\bar{1}1$	0.44	0.91	0.05
$10\bar{1}2$	0.42	--	0.36
$11\bar{2}0$	2.14	0.77	0.71
$10\bar{1}3$	0.79	--	1.19
$11\bar{2}2$	1.90	0.21	0.99
$20\bar{2}1$	0.44	2.20	--
$10\bar{1}4$	0.82	0	2.49
$20\bar{2}3$	0.33	0.08	0.13
$21\bar{3}0$	0.21	1.31	--
$21\bar{3}1$	1.05	0.80	0.10
$11\bar{2}4$	1.13	--	1.57
$21\bar{3}2$	0.70	0.33	--
$10\bar{1}5$	1.09	--	2.31
$21\bar{3}3$	1.21	0.11	0.20
$30\bar{3}2$	0.59	1.17	--
$20\bar{2}5$	1.40	--	0.72
$10\bar{1}6$	0.98	--	2.43
$21\bar{3}4$	1.19	--	0.61

778 228

7. HYDRIDE ORIENTATION

Zircaloy cladding picks up hydrogen during reactor operation, and the hydrides formed may precipitate in the undesirable radial direction. The hydrides oriented radially lie perpendicular to the maximum hoop stress and significantly reduce the ductility and strength of the cladding. F_n is the ratio of the number of hydrides oriented within 45^o of the radial direction, to the total number of hydrides, that is, it is a measure of the tendency of hydrides to precipitate in the radial direction. The F_n ratio also indicates the texture of the cladding. The hydrides precipitate on the basal planes; thus, the F_n ratio is an indication of the orientation of the basal planes, and the texture of the material.

Samples of PCM cladding were hydrided by electrolyzing in dilute H_2SO_4, and forming a thin layer of zirconium hydride on the specimen surface. The electrolyzed sample was annealed in a helium atmosphere to diffuse atomic hydrogen throughout the sample. Slow cooling to room temperature produced hydride platelets uniformly distributed in the zircaloy matrix. Figures 24 and 25 show photomicrographs of the hydride platelets in transverse and longitudinal sections of the tubing, respectively. The platelets are perpendicular to the radial direction in both figures. This result suggests that the basal poles are primarily aligned in the radial direction.

The F_n ratio was determined from the full circumference transverse sections shown in Figure 26. The wall thickness was divided into three equal counting zones representing outer, middle, and inner sections. Hydride platelets oriented within 45^o of the radial direction were defined as radial platelets. The F_n ratios for the outer, middle, and inner zones are 0.06, 0.03, and 0.05, respectively. An upper limit of 0.3 is usually specified for the F_n ratio.

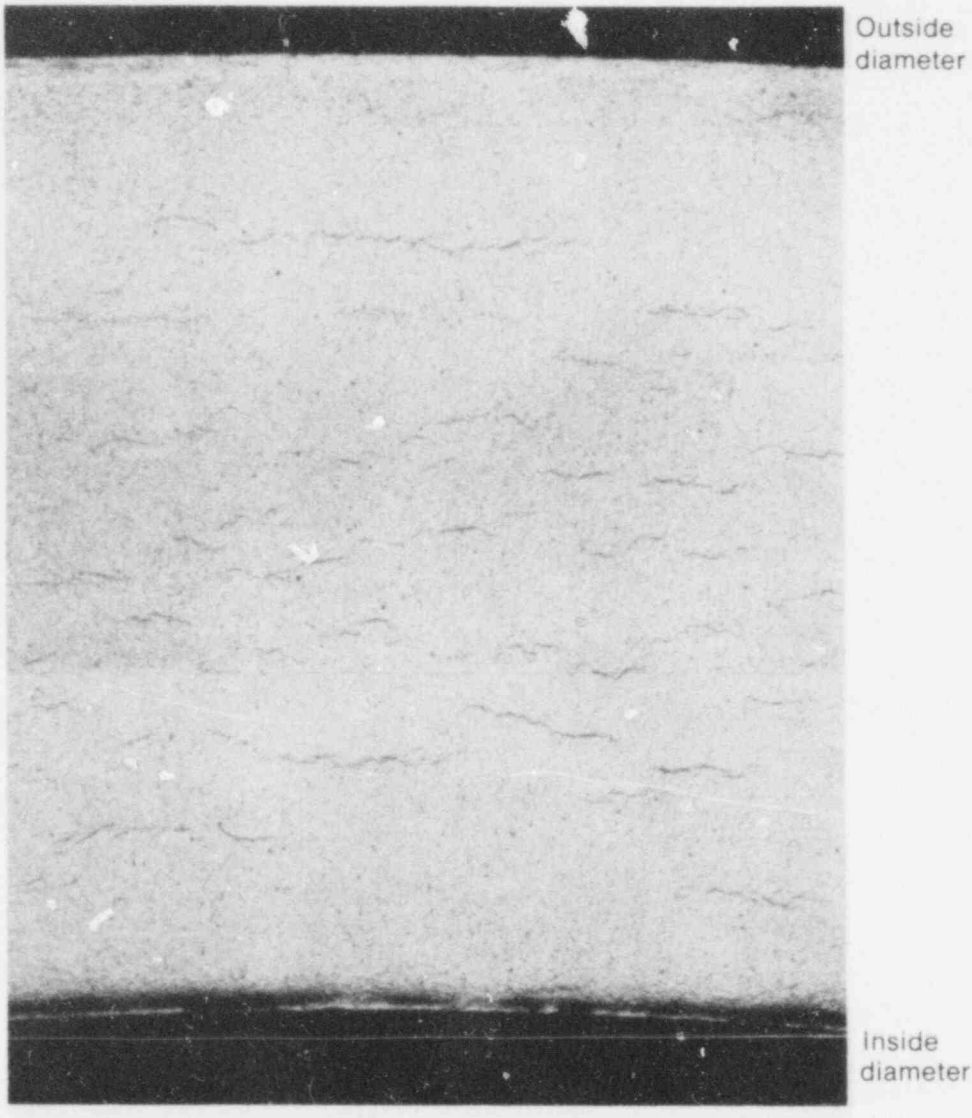

Fig. 24 PCM cladding hydride orientation (transverse section).

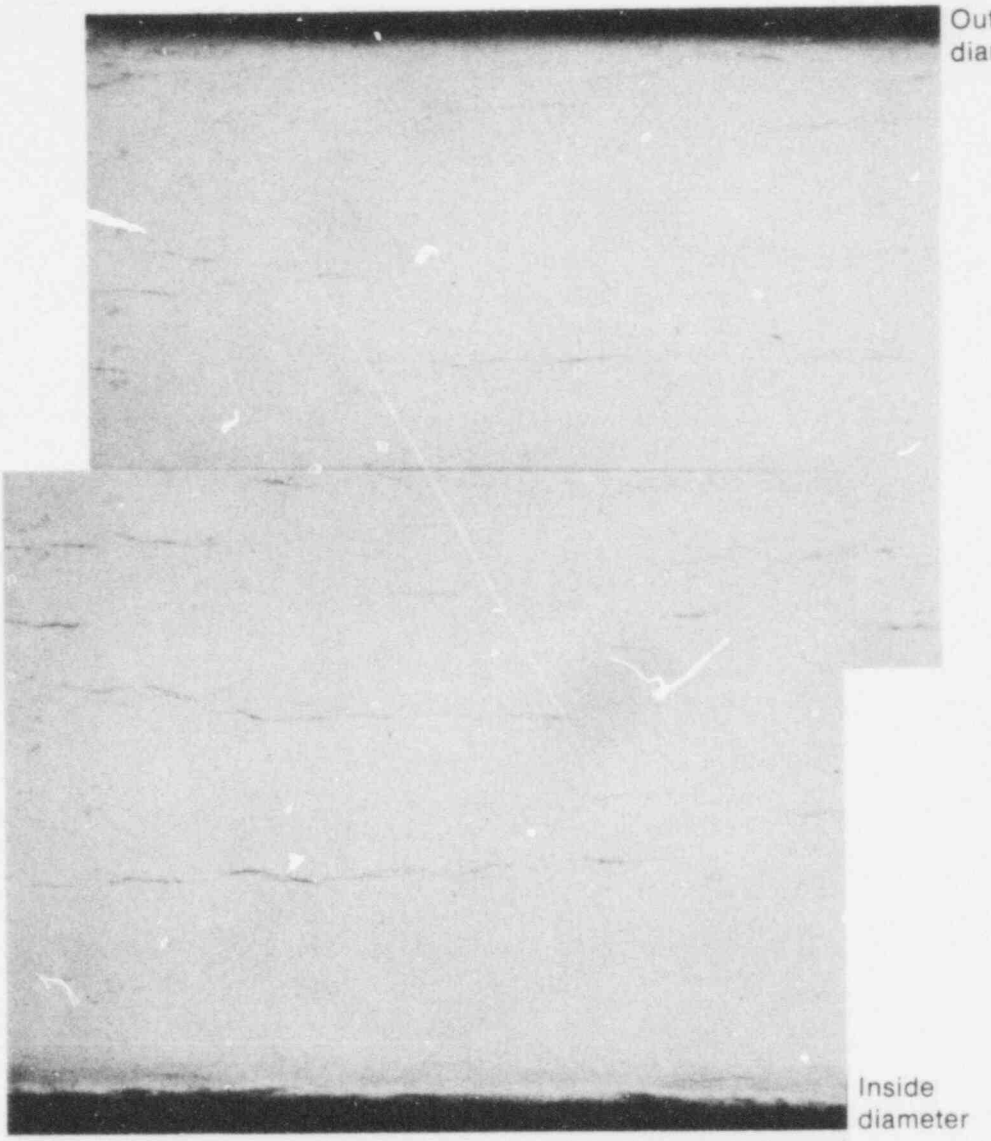

Fig. 25 PCM cladding hydride orientation (longitudinal section).

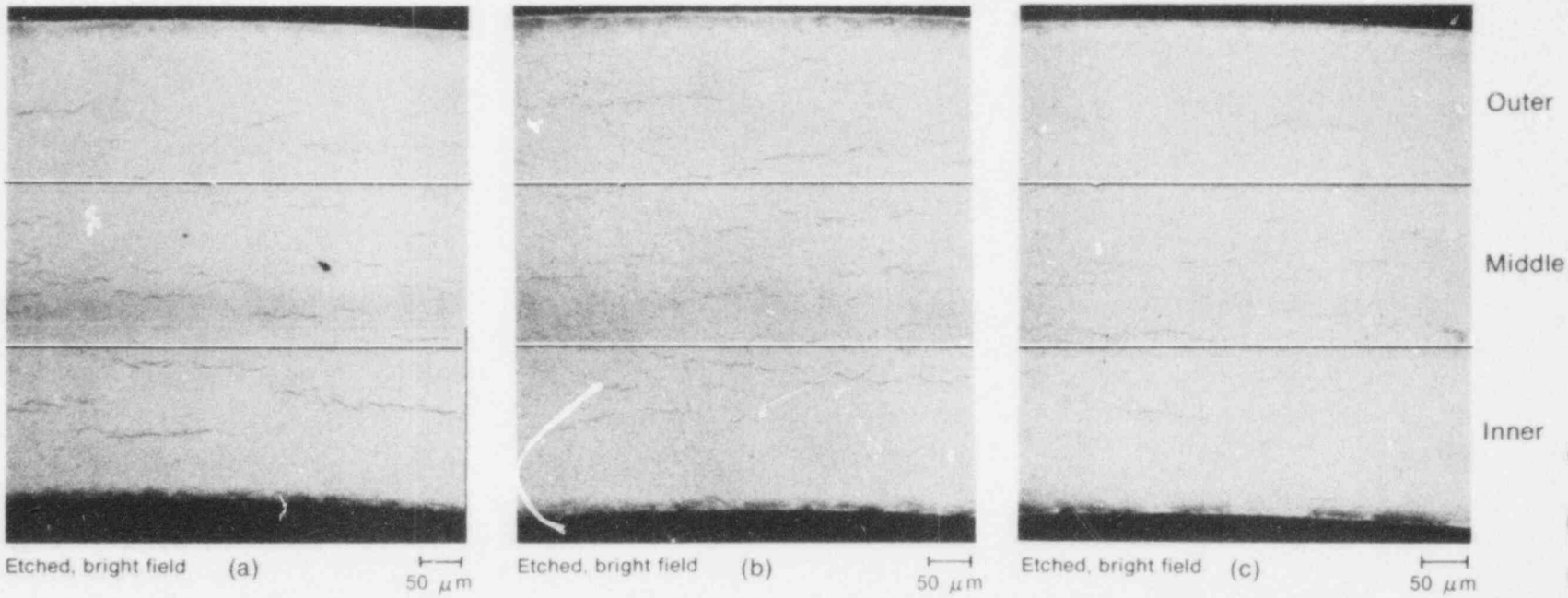

Fig. 26 PCM cladding hydride orientation (full circumference transverse sections).

III. FUEL CHARACTERIZATION

The UO_2 fuel fabricated for the PCM tests by Gulf United Nuclear Fuels Corporation, Chemical Operations[a], was made in three enrichments: 19.87% (Lot A-501-G29), 34.87% (Lot A-501-G32), and 93.16% (Lot A-501-G35). The fuel is characterized for each of these enrichments in the following sections: sintering conditions, physical dimensions, chemical analysis, microstructure, and density. The data reported in the following sections were provided by the fuel manufacturer, except where stated otherwise.

1. SINTERING CONDITIONS

Fuel pellet fabrication consisted of several steps. The UO_2 powder was first wet-milled and blended, then slugged and granulated. An organic lubricant (wax) was added to the granulated material and the mixture pressed into green compacts. (The wax binds the particles together in the compact, aids in controlling porosity, and lubricates the dies during pressing.) A presinter was used to remove the lubricant, followed by a final sintering to achieve the desired density. The pellet density was specified to be within the range 92 to 95% of theoretical density. The pellets were centerless ground to specified dimensions.

The temperature and times for the presinter are listed in Table VII. The atmosphere consisted of water-saturated NH_3 gas at 353 K, moving at 8.1 cm/s. The temperature and times were sufficient to remove the organic binder. Carbon analyses showed the carbon to be less than 10 ppm, compared with the 1 to 2% normally added to the green compacts.

The temperature and times for the sinter are listed in Table VIII. The 35 and 93% enriched pellets were sintered at relatively low temperatures (1773 to 1843 K). The 20% enriched pellets were sintered at slightly higher temperatures (1888 to 1913 K). The difference in sintering temperatures results in slightly different densities but significantly different porosity distributions which are discussed in Section III.4.2. The sintering atmosphere was water-saturated NH_3 gas at 353 K, moving at 3.2 cm/s.

TABLE VII

FUEL PELLET PRESINTERING CONDITIONS

	Lot A-501-G29 (20% enriched)	Lot A-501-G32 (35% enriched)	Lot A-501-G35 (93% enriched)
Temperature (K)	1193	1193	1193
Time at temperature (h)	1	2	1
Residence time (h)	5	10	5

[a] Gulf United Nuclear Fuels Corporation, Chemical Operations, Route 21-A, Hematite, Missouri 63047.

TABLE VIII

FUEL PELLET SINTERING CONDITIONS

	Lot A-501-G29 (20% enriched)	Lot A-501-G32 (35% enriched)	Lot A-501-G35 (93% enriched)
Temperature (K)	1888 to 1913	1773 to 1778	1843
Time at temperature (h)	3	2	3
Residence time (h)	7-1/2	5	7-1/2

2. PHYSICAL DIMENSIONS

Fuel pellet dimension specifications and measurements are given in Table IX, and were shown in Figure 2(b).

778 234

TABLE IX

FUEL PELLET DIMENSIONS

		Lot A-501-G29 (20% enriched)		Lot A-501-G32 (35% enriched)		Lot A-501-G35 (93% enriched)	
	Specification	Average	σ	Average	σ	Average	σ
Diameter (mm)	9.27 to 9.32	9.296	<0.01	9.296	0.005	9.296	0.003
Length (mm)	14.0 to 19.1	15.49	0.27	15.56	0.37	15.49	0.09
Dish depth (mm)	0.23 to 0.53	0.338	0.014	0.333	0.014	0.335	0.009
Land width (mm)	1.45 to 1.70	1.56	0.01	1.54	0.01	1.53	0.01
Calculated dish diameter (mm)	5.87 to 6.42	6.18		6.22		6.24	

3. CHEMICAL ANALYSIS

The UO_2 fuel U-235 content, oxygen-to-uranium (0:U) ratio, and gaseous impurity levels, including carbon, were determined for each fuel enrichment and are presented in Table X. Miscellaneous impurity levels are given in Table XI. The total of all impurities was specified to be less than 1500 ppm, with the total thermal neutron absorption cross section of all impurities not exceeding the equivalent of 4 ppm of boron. The total impurity levels for the three lots of fuel were well below the specified total level.

Moisture content of six whole pellets from each lot of fuel was determined just prior to tube loading (less than 12 hours before tube loading). The results are given in Table XII. The moisture contents are less than the specified maximum.

TABLE X

FUEL URANIUM CONTENT AND GASEOUS IMPURITY LEVELS (ppm)

	Specification	Lot A-501-G29[a] (20% enriched)	Lot A-501-G32[a] (35% enriched)	Lot A-501-G35[a] (93% enriched)
U-235 (wt%)	20, 35 and 93	19.856, 19.887	34.883, 34.858	93.167, 93.146
U (wt%)	87.9	88.07	88.04	87.97%
O:U	2.00:1 to 2.02:1	2.002, 2.002	2.000, 2.001	2.001, 2.001
C	<100	<10 ($<4.0\times10^{-5}$)	11 (4.4×10^{-5})	10 (4.0×10^{-5})
N	<100	25 (4.8×10^{-2})	14 (2.7×10^{-2})	56 (1.1×10^{-1})
Cl	<25	<10 ($<1.3\times10^{-1}$)	<5 ($<6.6\times10^{-2}$)	<5 ($<6.6\times10^{-2}$)
F	<25	13 (9.1×10^{-5})	21 (1.5×10^{-4})	14 (9.8×10^{-5})

[a] Values in parentheses for C, N, Cl, and F in each lot are boron equivalents. These values are included in impurity totals given in Table XI.

TABLE XI

FUEL IMPURITY ANALYSIS

Element	Lot A-501-G29 (20% enriched) ppm	Lot A-501-G29 (20% enriched) Boron Equivalent[a]	Lot A-501-G32 (35% enriched) ppm	Lot A-501-G32 (35% enriched) Boron Equivalent[a]	Lot A-501-G35 (93% enriched) ppm	Lot A-501-G35 (93% enriched) Boron Equivalent[a]
Al	<10	$<1.2 \times 10^{-3}$	<10	$<1.2 \times 10^{-3}$	<10	$<1.2 \times 10^{-3}$
B	<0.1	$<1.0 \times 10^{-1}$	<0.1	$<1.0 \times 10^{-1}$	<0.1	$<1.0 \times 10^{-1}$
Ca	<5	$<7.7 \times 10^{-4}$	<5	$<7.7 \times 10^{-4}$	<5	$<7.7 \times 10^{-4}$
Cd	<0.2	$<6.5 \times 10^{-2}$	<0.2	$<6.5 \times 10^{-2}$	<1	$<3.3 \times 10^{-1}$
Cr	10	8.0×10^{-3}	10	8.0×10^{-3}	<10	$<8.0 \times 10^{-3}$
Co	<1	$<9.2 \times 10^{-3}$	<1	$<9.2 \times 10^{-3}$	<5	$<4.6 \times 10^{-2}$
Cu	<5	$<4.3 \times 10^{-3}$	<5	$<4.3 \times 10^{-3}$	<1	$<8.7 \times 10^{-4}$
Fe	68	4.6×10^{-2}	77	5.2×10^{-2}	26	1.7×10^{-2}
Pb	<1	$<1.1 \times 10^{-5}$	1	1.1×10^{-5}	1	1.1×10^{-5}
Li	<1	$<1.5 \times 10^{-1}$	4	$<1.5 \times 10^{-1}$	<1	$<1.5 \times 10^{-1}$
Mg	10	4.0×10^{-4}	10	4.0×10^{-4}	<1	$<4.0 \times 10^{-5}$
Mn	<5	$<1.7 \times 10^{-2}$	<5	$<1.7 \times 10^{-2}$	<1	$<3.4 \times 10^{-3}$
Mo	10	$<4.0 \times 10^{-3}$	<10	$<4.0 \times 10^{-3}$	<10	$<4.0 \times 10^{-3}$

TABLE XI (continued)

Element	Lot A-501-G29 (20% enriched) ppm	Boron Equivalent[a]	Lot A-501-G32 (35% enriched) ppm	Boron Equivalent[a]	Lot A-501-G35 (93% enriched) ppm	Boron Equivalent[a]
Ni	65	7.3×10^{-2}	34	3.8×10^{-2}	111	1.2×10^{-1}
P	<20	$<1.7 \times 10^{-3}$	<20	$<1.7 \times 10^{-3}$	<20	$<1.7 \times 10^{-3}$
Si	<10	$<6.6 \times 10^{-4}$	<10	$<6.6 \times 10^{-4}$	<10	$<6.6 \times 10^{-4}$
Ag	<0.1	$<8.2 \times 10^{-4}$	<0.1	$<8.2 \times 10^{-4}$	<0.1	$<8.2 \times 10^{-4}$
Na	10	2.5×10^{-3}	10	2.5×10^{-3}	10	2.5×10^{-3}
Th	<5	$<2.3 \times 10^{-3}$	<5	$<2.3 \times 10^{-3}$	<5	$<2.3 \times 10^{-3}$
Sn	2	1.4×10^{-4}	5	3.6×10^{-4}	<5	$<3.6 \times 10^{-4}$
W	<10	$<1.5 \times 10^{-2}$	50	7.5×10^{-2}	<10	$<1.5 \times 10^{-2}$
Ti	<1	$<2.4 \times 10^{-4}$	<1	$<2.4 \times 10^{-4}$	<1	$<2.4 \times 10^{-4}$
V	<1	$<1.4 \times 10^{-3}$	<1	$<1.4 \times 10^{-3}$	<1	$<1.4 \times 10^{-3}$
Zn	<5	$<1.2 \times 10^{-3}$	<5	$<1.2 \times 10^{-3}$	<1	$<2.4 \times 10^{-4}$
Zr	<50	$<1.5 \times 10^{-3}$	<10	$<2.9 \times 10^{-4}$	<50	$<1.5 \times 10^{-3}$
Sm	<0.1	$<5.2 \times 10^{-2}$	<0.1	$<5.2 \times 10^{-2}$	<0.1	$<5.2 \times 10^{-2}$
Eu	<0.1	$<4.3 \times 10^{-2}$	<0.1	$<4.3 \times 10^{-2}$	<0.1	$<4.3 \times 10^{-2}$

TABLE XI (continued)

Element	Lot A-501-G29 (20% enriched) ppm	Lot A-501-G29 (20% enriched) Boron Equivalent[a]	Lot A-501-G32 (35% enriched) ppm	Lot A-501-G32 (35% enriched) Boron Equivalent[a]	Lot A-501-G35 (93% enriched) ppm	Lot A-501-G35 (93% enriched) Boron Equivalent[a]
Gd	<0.1	$<4.2 \times 10^{-1}$	<0.1	$<4.2 \times 10^{-1}$	<0.1	$<4.2 \times 10^{-1}$
Dy	<0.1	$<9.7 \times 10^{-3}$	<0.1	$<9.7 \times 10^{-3}$	<0.1	$<9.7 \times 10^{-3}$
Total[b]	<363.8	<1.21	<337.8	<1.15	<381.6	<1.51

[a] The term "boron equivalent" is defined as the neutron capture characteristic of one ppm of that element compared with the neutron capture characteristic of one ppm of boron.

[b] Includes gaseous impurities from Table X.

TABLE XII

FUEL PELLET MOISTURE CONTENT (ppm H_2O)

	Specification	Lot A-501-G29 (20% enriched)	Lot A-501-G32 (35% enriched)	Lot A-501-G35 (93% enriched)
Six Pellets		2.6, 1.2, 0.9, 0.6, 7.4, 5.6	3.2, 6.8, 7.1, 6.0, 1.3, 1.7	1.7, 2.4, 2.7, 1.1, 1.4, 1.3
Average		3.1	4.4	1.8
Maximum	25	7.4	7.1	2.7

4. MICROSTRUCTURE

The microstructure and fracture surfaces were characterized for each of the three UO_2 fuel enrichments. One pellet of each enrichment was fractured transversely by supporting the ends in a V-block and striking the middle of the pellet. One-half of each fractured pellet was mounted for optical microscopic examination, and the fracture surface of the other half was examined with the scanning electron microscope. Fuel grain size, pore size and distribution, and fractography are discussed in the following sections.

4.1 Grain Size

Fuel grain sizes were reported by the fuel manufacturer for a transverse and a longitudinal section of each fuel enrichment. The values are given in Table XIII. Radial distribution of the fuel grain size was determined at EG&G Idaho, Inc., for one pellet of each fuel enrichment, using the intercept method to approximate the fuel grain diameters. The results are given in Table XIV. The grain sizes reported by the fuel manufacturer and EG&G Idaho, Inc., are about equal. Etched fuel photomicrographs prepared at EG&G Idaho, Inc., showing fuel grain sizes for the 20, 35, and 93% enriched fuel lots are presented in Figures 27, 28, and 29, respectively.

4.2 Pore Size and Distribution

Pore sizes were determined from one transverse and one longitudinal sample of each enrichment by the fuel manufacturer. The pores were counted in the following groups:

<0.5 μm - not counted
0.5 to 1 μm
1 to 1.5 μm
1.5 to 2 μm
>2 μm - measured to nearest 0.5.

The results are summarized in Table XV.

Pore distribution was determined at EG&G Idaho, Inc., for one pellet of each enrichment. High magnification unetched fuel photomicrographs prepared at EG&G Idaho, Inc., are presented in Figures 30, 31, and 32 for the 20, 35, and 93% enriched fuel lots, respectively. As can be seen in Figure 30, most of the 20% enriched fuel pores appear randomly distributed but a few appear to be located along boundaries (probably grain boundaries). Most of the 35 and 93% enriched fuel pores, however, appear to be located along these boundaries (Figures 31 and 32). This difference in microstructure may be related to the higher sintering temperature of the 20% enriched fuel (~1900 K compared with 1773 and 1843 K for the 35 and

TABLE XIII

FUEL GRAIN SIZES

	Grain Size (μm)	
	Transverse Section	Longitudinal Section
Lot A-501-G29 (20% enriched)	4.3	5.8
	3.7	4.3
	3.7	4.1
	3.6	5.1
	3.2	5.5
	3.9	4.1
	3.6	4.3
	4.3	3.9
	3.3	3.7
	4.1	4.8
	Average 3.7	Average 4.5
Lot A-501-G32 (35% enriched)	4.1	3.4
	3.7	3.9
	4.3	4.6
	4.1	3.7
	3.4	4.3
	4.6	5.1
	3.9	4.1
	3.9	3.4
	3.6	3.7
	4.3	3.7
	Average 4.0	Average 4.0
Lot A-501-G35 (93% enriched)	3.6	3.6
	3.3	3.2
	3.4	3.3
	3.3	3.3
	3.1	3.2
	3.4	3.0
	3.6	3.4
	3.3	3.3
	3.3	3.2
	3.7	3.7
	Average 3.4	Average 3.3

TABLE XIV

FUEL GRAIN SIZE RADIAL DISTRIBUTIONS[a]

	Grain Size (μm)		
	Edge	Midradius	Center
Lot A-501-G29 (20% enriched)	3.5	5.5	3.8
Lot A-501-G32 (35% enriched)	2.5	2.3	2.3
Lot A-501-G35 (93% enriched)	2.3	2.5	2.9

[a] Measurements made at EG&G Idaho, Inc.

93% enriched fuel lots). Sintering times and temperatures for the three enrichments were given in Table VIII.

4.3 Fractography

Fracture surfaces of one fuel pellet of each enrichment were examined using the scanning electron microscope (SEM). Figures 33, 34, and 35 each show a photomacrograph of the pellet transverse fracture surface with a higher magnification SEM composite across one diameter, for the 20, 35, and 93% fuel enrichments, respectively. Figures 36 through 40 show specific areas of the three fracture surfaces at higher magnification, taken on the SEM. At present, how to relate the appearance and characteristics of out-of-reactor mechanically-produced fractures to in-reactor thermally-induced fractures is not clear.

778 243

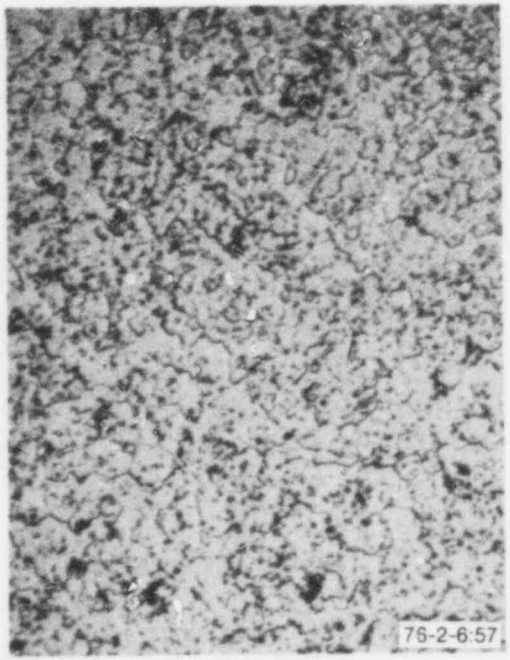

(a) Edge of fuel pellet
Grain size 3.5 μm

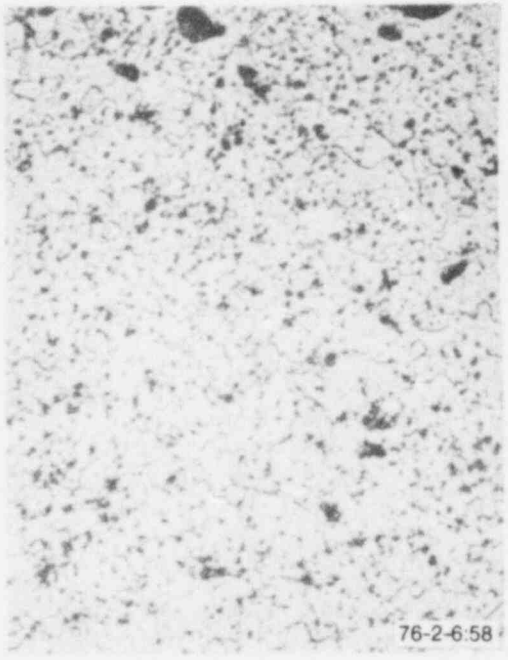

(b) Midradius of fuel pellet
Grain size 5.5 μm

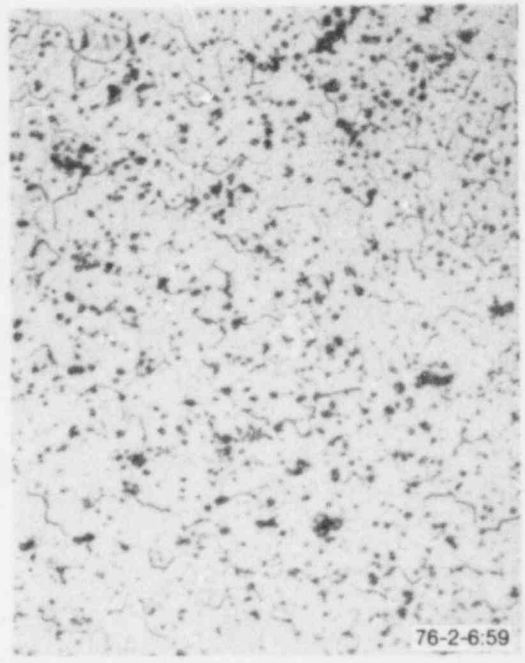

(c) Center of fuel pellet
Grain size 3.8 μm

GS-008-6

Fig. 27 Grain sizes of 20% enriched fuel pellet.

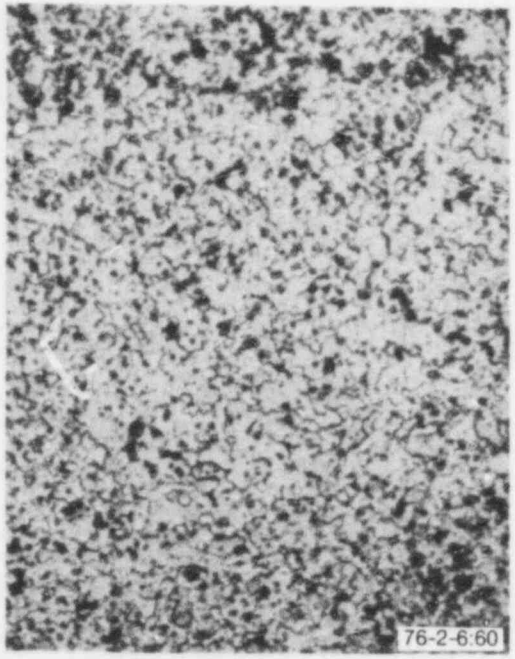

(a) Edge of fuel pellet
Grain size 2.5 μm

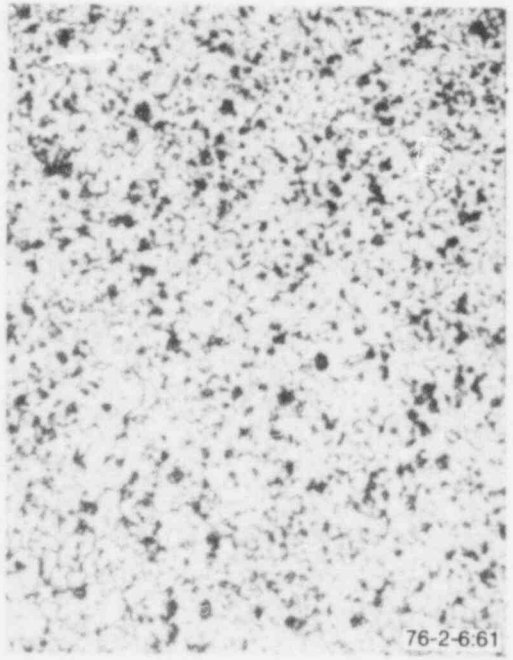

(b) Midradius of fuel pellet
Grain size 2.3 μm

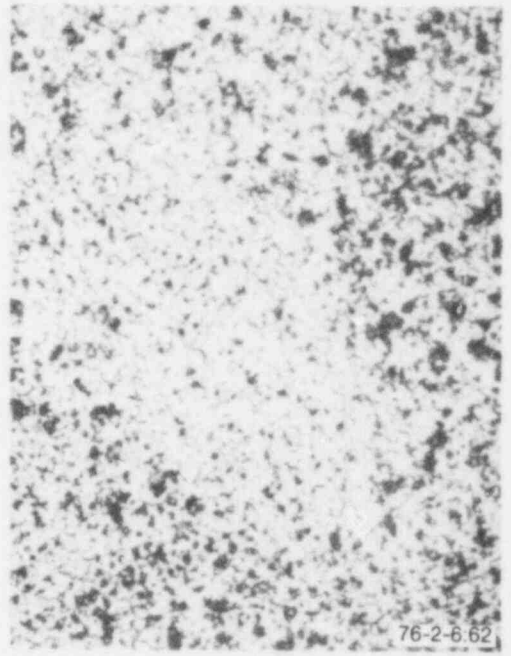

(c) Center of fuel pellet
Grain size 2.3 μm

GS-008-7

Fig. 28 Grain sizes of 35% enriched fuel pellet.

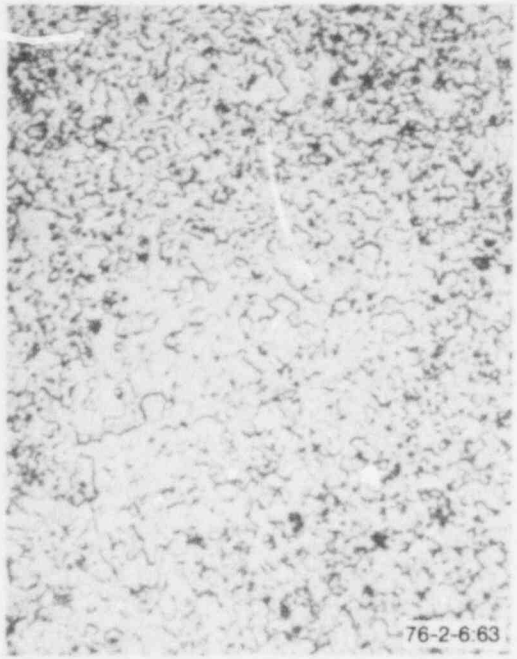

Etched, bright field — 40 μm

(a) Edge of fuel pellet
Grain size 2.3 μm

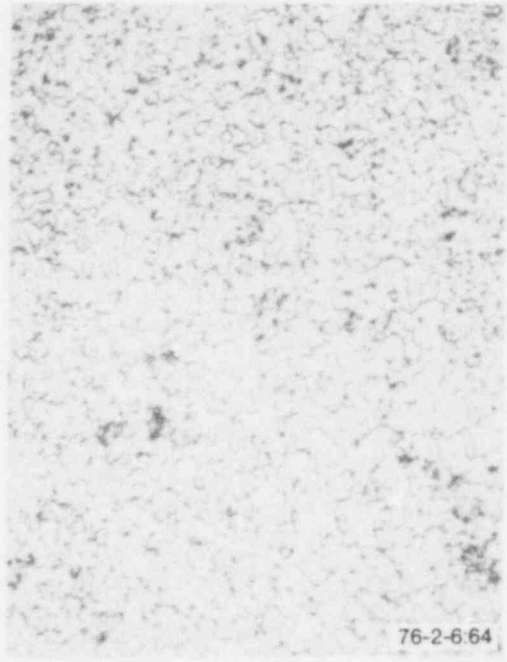

Etched, bright field — 40 μm

(b) Midradius of fuel pellet
Grain size 2.5 μm

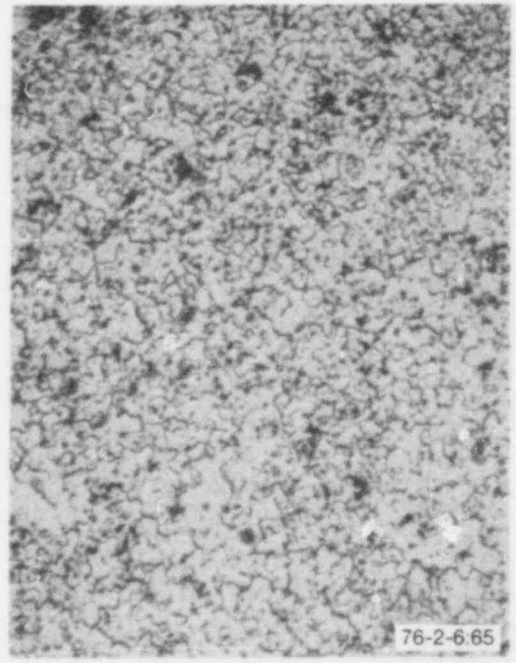

Etched, bright field — 40 μm

(c) Center of fuel pellet
Grain size 2.9 μm

GS-008-11

Fig. 29 Grain sizes of 93% enriched fuel pellet.

TABLE XV

FUEL PORE SIZES

			Pore Size (μm)				
			0.5 to 1	1 to 1.5	1.5 to 2	>2 (average diameter)	Total
Lot A-501-G29 (20% enriched)	Transverse section	Number of pores	167	20	11	14 (3.21)	212
		Weighted composite[a]	0.591	0.118	0.091	0.212	
		Average pore diameter	- - - - - - - (for all sizes) 1.012 - - - - - -				
	Longitudinal section	Number of pores	78	22	10	21 (2.79)	131
		Weighted composite[a]	0.447	0.210	0.134	0.447	
		Average pore diameter	- - - - - - - (for all sizes) 1.238 - - - - - - -				
Lot A-501-G32 (35% enriched)	Transverse section	Number of pores	281	58	11	11 (3.23)	361
		Weighted composite[a]	0.584	0.201	0.053	0.098	
		Average pore diameter	- - - - - - - (for all sizes) 0.936 - - - - - - -				
	Longitudinal section	Number of pores	58	12	7	17 (3.41)	94
		Weighted composite[a]	0.463	0.160	0.130	0.617	
		Average pore diameter	- - - - - - - (for all sizes) 1.370 - - - - - - -				
Lot A-501-G35 (93% enriched)	Transverse section	Number of pores	192	33	6	14 (3.39)	245
		Weighted composite[a]	0.588	0.168	0.043	0.194	
		Average pore diameter	- - - - - - - (for all sizes) 0.993 - - - - - - -				
	Longitudinal section	Number of pores	81	25	8	13 (3.19)	127
		Weighted composite[a]	0.478	0.246	0.110	0.327	
		Average pore diameter	- - - - - - - (for all sizes) 1.161 - - - - - - -				

[a] The average pore size for each group was assumed to be the range midpoint. The weighted composite was calculated by multiplying the fractional number of pores by the range midpoint, for example, 0.75μm x 167/212 = 0.591.

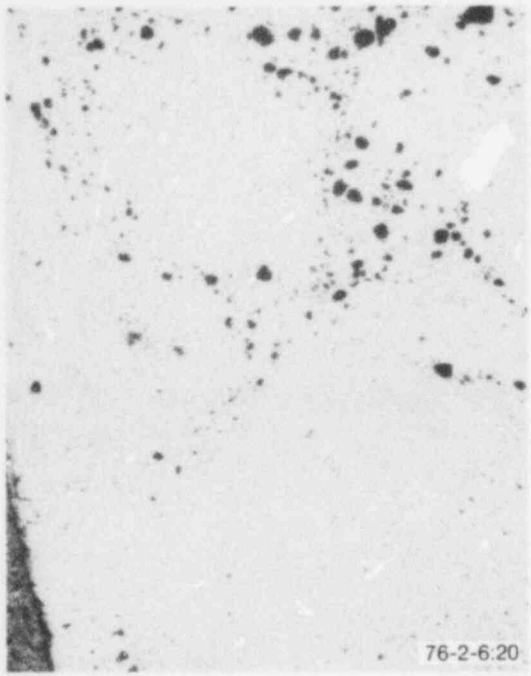

(a) Edge of fuel pellet

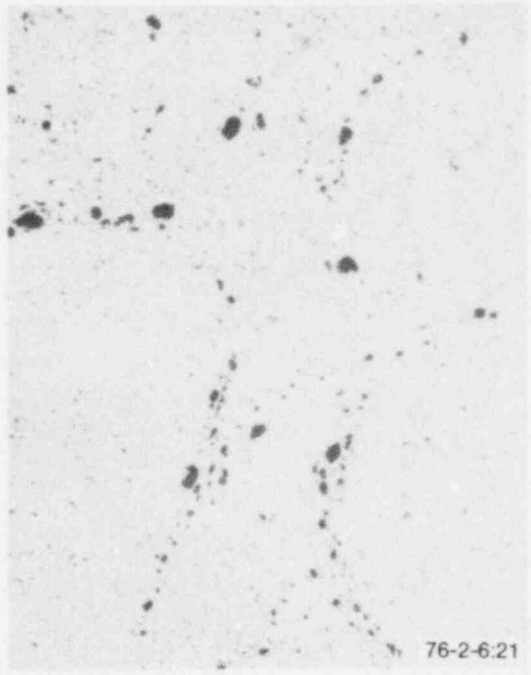

(b) Midradius of fuel pellet

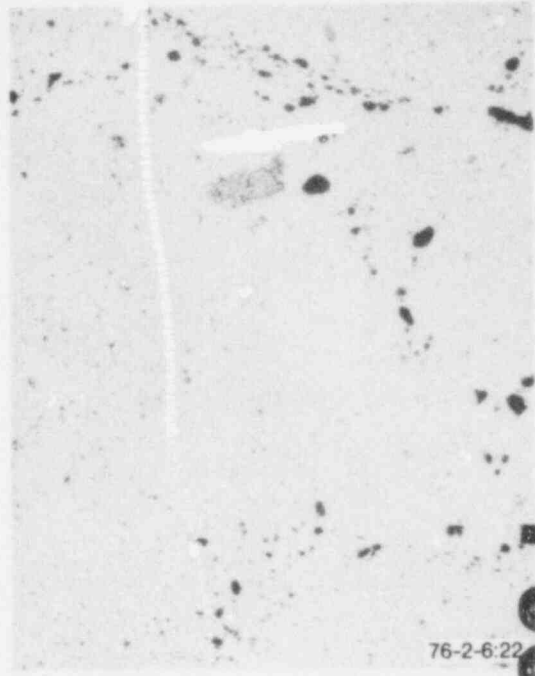

(c) Center of fuel pellet

GS-008-8

Fig. 30 Porosity of 20% enriched fuel pellet.

As-polished

1 μm

(a) Edge of fuel pellet

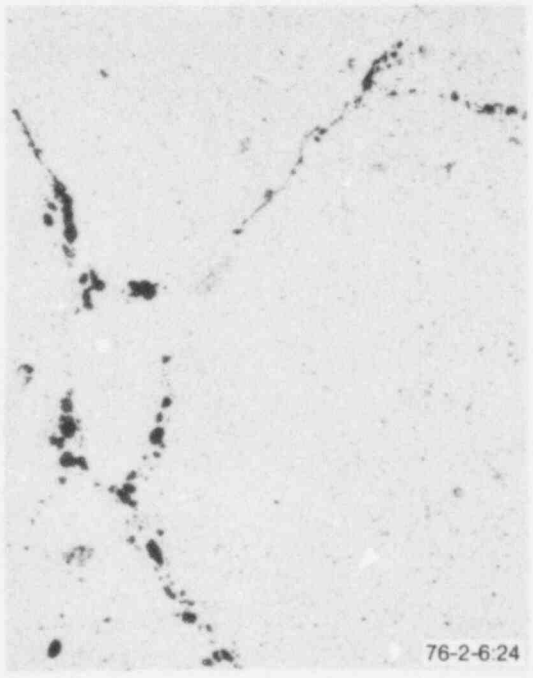

As-polished

1 μm

(b) Midradius of fuel pellet

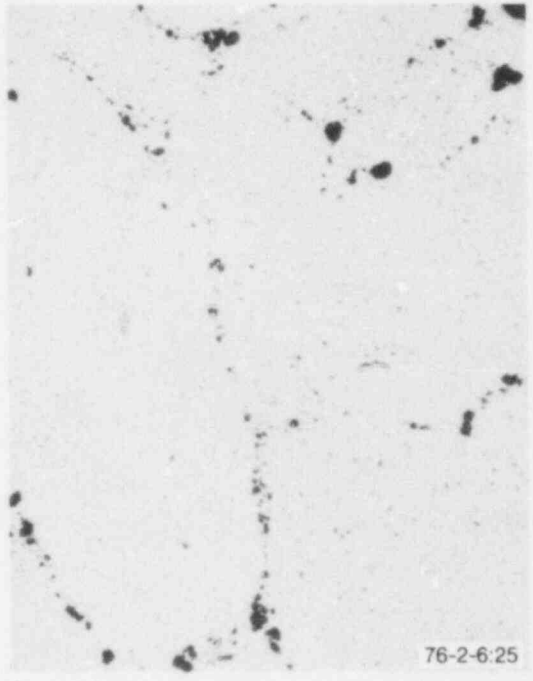

As-polished

1 μm

(c) Center of fuel pellet

GS-008-9

Fig. 31 Porosity of 35% enriched fuel pellet.

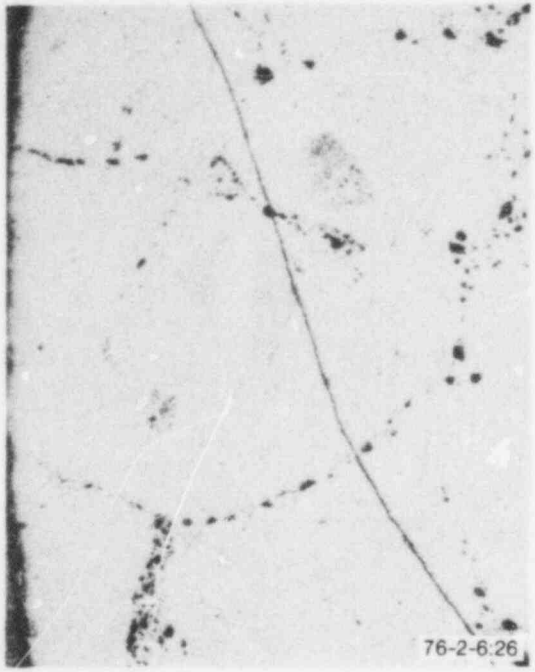

(a) Edge of fuel pellet

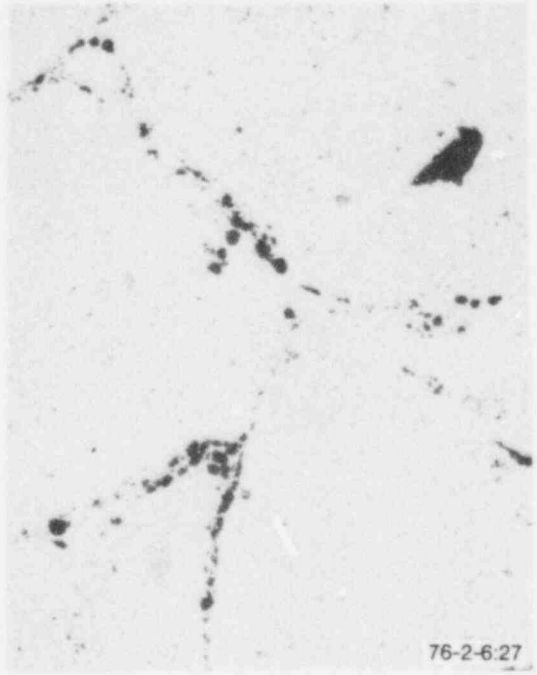

(b) Midradius of fuel pellet

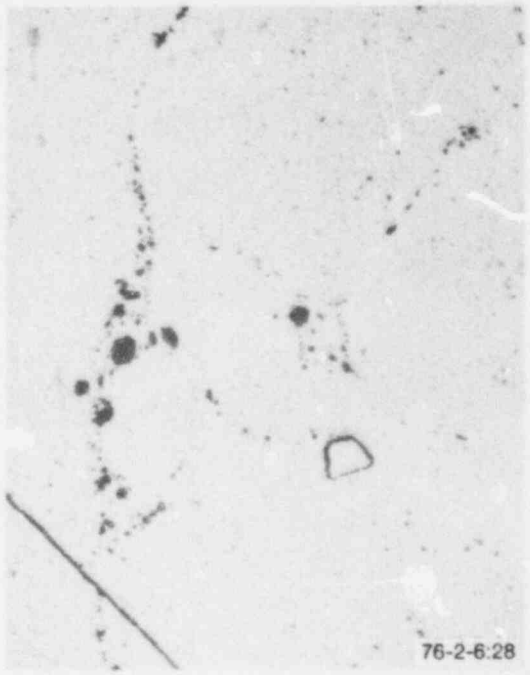

(c) Center of fuel pellet

GS-008-10

Fig. 32 Porosity of 93% enriched fuel pellet.

DOCUMENT/ PAGE PULLED

ANO. 7908240068

NO. OF PAGES 8

REASON:

☒ PAGE ILLEGIBLE:

☐ HARD COPY FILED AT: PDR (CF)

OTHER _____

☐ BETTER COPY REQUESTED ON ____/____/____

☐ PAGE TOO LARGE TO FILM:

☐ HARD COPY FILED AT: PDR CF

OTHER _____

☐ FILMED ON APERTURE CARD NO. _____

5. DENSITY

Immersion density measurements were performed at EG&G Idaho, Inc., on the fuel samples used for the fracture surface studies of the preceding section, after completion of that work. The immersion density of a fuel sample is determined to within ± 0.001 g/cm^3 by the following method:

(1) The dry weight (W_D) of the pellet is determined to within ± 0.001 g.

(2) The pellet is placed in a small water-filled vial. The vial with pellet is put in a vacuum desiccator, which is connected to a cold trap and a mechanical vacuum pump.

(3) The system is pumped out for 30 minutes, evacuating the air above the surface of the water and removing the open porosity on the surface of the pellet.

(4) The vial is removed and the immersion weight (W_I) of the pellet suspended in water is determined.

(5) The water temperature is measured to determine the density of the water (D_{H_2O}).

(6) The pellet is taken out of the vial and the surface moisture is removed by rolling the pellet on a lint-free towel saturated with water.

(7) The pellet is weighed to determine the saturated weight (W_S).

(8) The pellet density (D_P) is calculated from

$$D_P = \frac{W_D \cdot D_{H_2O}}{W_S - W_I} .$$

The immersion density results for the three samples are given in Table XVI.

TABLE XVI

FUEL IMMERSION DENSITIES

	Lot A-501-G29 (20% enriched)	Lot A-501-G32 (35% enriched)	Lot A-501-G35 (93% enriched)
Density (g/cm^3)	10.320 $\pm$ 0.001	10.228 $\pm$ 0.001	10.177 $\pm$ 0.001
Percent of theoretical density (10.96 g/cm^3)	94.16 $\pm$ 0.01	93.32 $\pm$ 0.01	92.86 $\pm$ 0.01

Resintering tests were performed at EG&G Idaho, Inc., to determine the densification stability of the fuel. Eight fuel pellets from Lot A-501-G29 (20% enriched) were resintered at 2070 K in a reducing atmosphere (argon - 8% hydrogen) for six two-hour cycles. Immersion density measurements were made before the tests began, and after each two-hour cycle, on each fuel pellet. The average immersion density of the eight pellets as-received and after each cycle are given in Table XVII and shown in Figure 41. Significant fuel densification occurred. The maximum measured increase in density was 0.3 g/cm^3 or approximately 3% of theoretical density (10.96 g/cm^3). As can be seen from Figure 41, the densification tends to saturate at approximately 10.70 g/cm^3 or 97.6% of theoretical density.

TABLE XVII

AVERAGE IMMERSION DENSITY OF EIGHT 20% ENRICHED FUEL PELLETS AFTER RESINTERING TESTS

	Average Density	
	g/cm^3	percent of theoretical
As-received	10.35 ± 0.04	94.43 ± 0.36
Cycle 1	10.48 ± 0.03	95.62 ± 0.27
Cycle 2	10.58 ± 0.04	96.53 ± 0.36
Cycle 3	10.61 ± 0.03	96.81 ± 0.27
Cycle 4	10.62 ± 0.05	96.90 ± 0.46
Cycle 5	10.66 ± 0.04	97.26 ± 0.36
Cycle 6	10.65 ± 0.03	97.17 ± 0.27

778 253

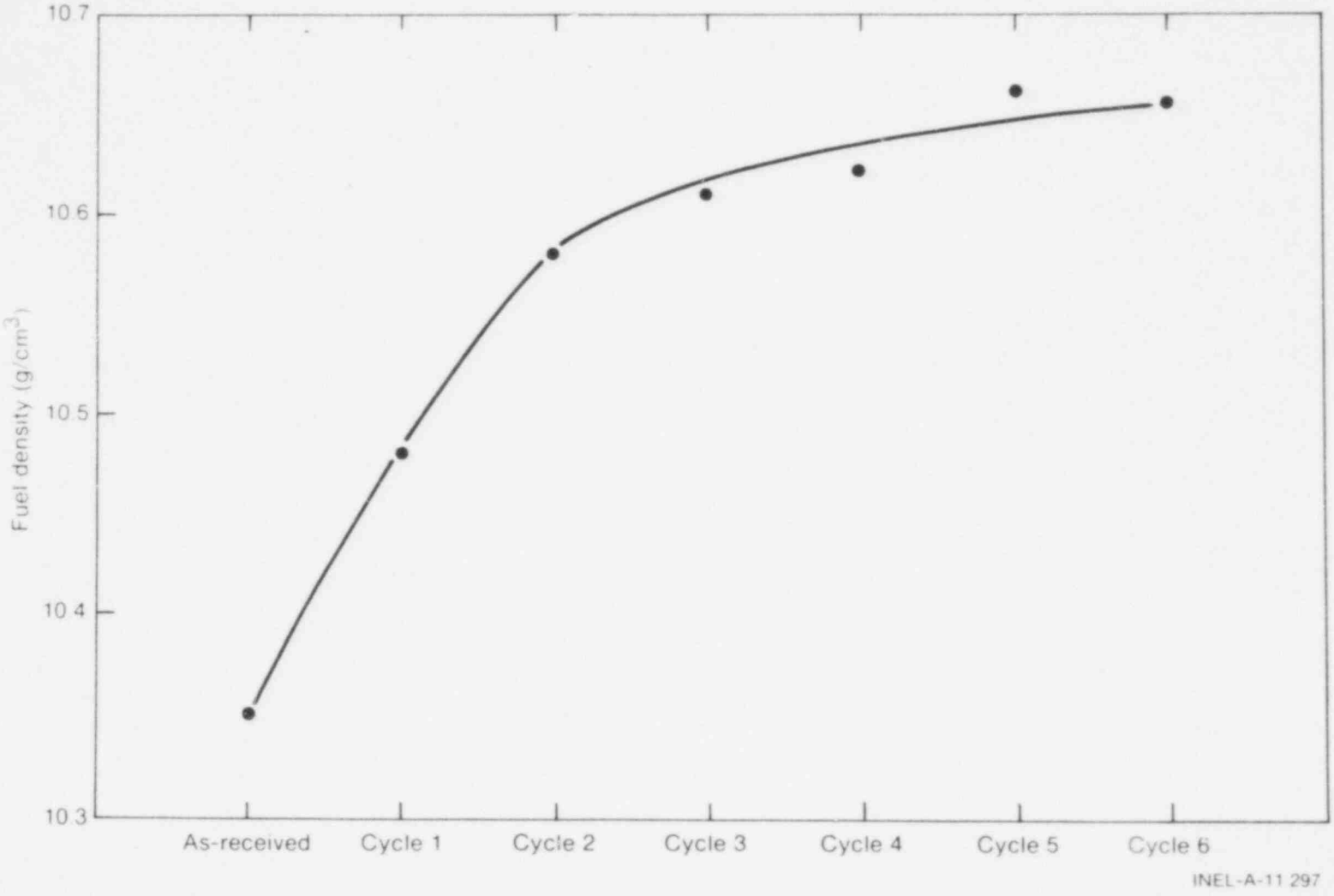

Fig. 41 Average immersion density of eight PCM fuel pellets (20% enriched) after resintering tests.

IV. END CAP CHARACTERIZATION

The PCM fuel rod top and bottom end caps were made by a Gulf United Nuclear Fuels Corporation approved vendor from zircaloy-2 rod stock manufactured by Wah Chang Albany Corporation[a] according to ASTM B351-67 specifications (Type RA-1). The top and bottom end cap dimensions were given in Figure 2(c). The following sections discuss end cap chemical analysis, and tensile properties and hardness.

1. CHEMICAL ANALYSIS

Chemical analyses of the zircaloy-2 ingot and rod stock were supplied by the rod stock manufacturer (Wah Chang Albany Corporation) and are given in Tables XVIII and XIX, respectively. Table XX presents the end cap chemical analysis performed by the fuel rod manufacturer (Gulf United Nuclear Fuels Corporation). The oxygen content was specified to be less than 1400 ppm. The chemical composition and impurity levels are within the specified ranges.

778 255

[a] Wah Chang Albany Corporation, P.O. Box 460, Albany, Oregon 97312.

TABLE XVIII

ZIRCALOY-2 END CAP ROD STOCK INGOT ANALYSIS PERFORMED BY ROD STOCK MANUFACTURER

	Composition (%)		
	Specification	Top	Bottom
Sn	1.20 to 1.70	1.47	1.39
Fe	0.07 to 0.20	0.17	0.15
Cr	0.05 to 0.15	0.10	0.10
Ni	0.03 to 0.08	0.06	0.05
	Impurities (ppm)		
Al	<75	44	38
B	<0.5	0.2	0.2
C	<270	150	150
Ca	--	<10	<10
Cd	<0.5	<0.2	<0.2
Cl	--	<15	<15
Co	<20	<5	<5
Cu	<50	14	10
H_2	<25	2.4	6
Hf	<100	130	115
Mg	<20	<5	<5
Mn	<50	<10	<10
Mo	<50	<10	<10
N_2	<80	41	51
Nb	--	<100	<100
O_2	<1400	1050	1360
Pb	--	<20	<20

TABLE XVIII (continued)

	Impurities (ppm) (continued)		
	Specification	Top	Bottom
Si	<120	76	67
Ta	--	<200	<200
Ti	--	<15	<15
U	<3.5	1.1	1.2
V	--	<5	<5
W	<100	<25	<25

TABLE XIX

ZIRCALOY-2 END CAP ROD STOCK ANALYSIS PERFORMED BY ROD STOCK MANUFACTURER (ppm)

	Specification	Sample 1	Sample 2
H_2	<25	5	6
N_2	<80	51	52
O_2	<1400	1090	1170

TABLE XX

ZIRCALOY-2 END CAP ANALYSIS PERFORMED BY FUEL ROD MANUFACTURER (ppm)

	Specification	Sample 1	Sample 2
H_2	<25	7	9
N_2	<80	48	46
O_2	<1400	1270	1090
		1150	1300

778 25

2. TENSILE PROPERTIES AND HARDNESS

Tensile properties of the end cap rod stock were determined at room temperature by the rod stock manufacturer and are presented in Table XXI. Ingot hardness analysis results provided by the rod stock manufacturer are also given in Table XXI.

TABLE XXI

ZIRCALOY-2 END CAP ROD STOCK TENSILE PROPERTIES AT ROOM TEMPERATURE AND INGOT HARDNESS ANALYSIS PROVIDED BY THE ROD STOCK MANUFACTURER

Sample	Yield Strength (MPa)	Ultimate Tensile Strength (MPa)	Elongation (%)
1	343	533	25.0
2	340	530	30.0
		Hardness (BHN)	
		Range 170 to 179	
		Average 175	

778 253

V. ALUMINA SPACER CHARACTERIZATION

Alumina (Al_2O_3) disks used as fuel stack spacers in the PCM rods were manufactured by Coors/Spectro-Chemical Laboratory[a]. The alumina spacer dimensions were given in Figure 2(d). The following sections discuss alumina spacer chemical analysis; porosity and absorption; and density, compressive strength, and hardness.

1. CHEMICAL ANALYSIS

Chemical analyses of three samples were performed by the spacer manufacturer. The results with specifications are presented in Table XXII.

TABLE XXII

ALUMINA SPACER ANALYSIS PERFORMED BY SPACER MANUFACTURER (wt%)

		Sample		
	Specification	1	2	3
SiO_2	<0.2	0.2	0.2	0.2
Fe_2O_3	--	0.04	0.05	0.05
CaO	--	0.2	0.1	0.1
MgO	<1.0	0.2	0.2	0.2
Na_2O	--	0.008	0.008	0.008
TiO_2	--	0.005	0.005	0.005
Cl	<0.005	0.0013	0.0016	0.0016
F	<0.005	<0.0002	<0.0002	<0.0002
Al_2O_3	>99.0	99.35[a]	99.44[a]	99.44[a]

[a] By difference.

[a] Coors/Spector-Chemical Laboratory, Division of Coors Porcelain Company, Golden, Colorado.

2. POROSITY AND ABSORPTION

Fifteen samples were tested for porosity and absorption by the spacer manufacturer using dye penetrant DP-50 Red Water Washable Penetrant Liquid manufactured by Belmont Chemicals Division of Sherwin, Inc. The samples were immersed in the dye penetrant, pressurized in a chamber to 5.52 MPa for one hour, and the excess liquid washed from the surfaces. No pink or red color remained, that is, these samples passed specification MIL-I-25135C, Group III.

3. DENSITY, COMPRESSIVE STRENGTH, AND HARDNESS

Density, compressive strength, and hardness of three samples were measured by the spacer manufacturer according to specifications ASTM D116-69, ASTM C528-63T, and ASTM E18-67, respectively. The results with specifications are presented in Table XXIII.

TABLE XXIII

ALUMINA SPACER DENSITY, COMPRESSIVE STRENGTH, AND HARDNESS MEASURED BY SPACER MANUFACTURER

		Sample		
	Specification	1	2	3
Density (g/cm^3)	>3.70	3.91	3.90	3.90
Compressive strength (MPa)	>2068.25	2572.03	2166.74	2745.36
Hardness (Rockwell 45N)	>80	84.1	84.3	84.3

VI. COMPRESSION SPRING CHARACTERIZATION

Compression springs used at the top of the fuel stack in the PCM rods were fabricated by Gulf United Nuclear Fuels Corporation from wire manufactured by New England High Carbon Wire Corporation[a]. The oil tempered chromium vanadium alloy spring wire was made according to specification ASTM A231-68. The spring dimensions were given in Figure 2(e), and the spring wire chemical analysis, determined by the wire manufacturer, is given in Table XXIV. The wire tensile strength ranged between 2013.10 and 2068.25 MPa.

TABLE XXIV

COMPRESSION SPRING WIRE ANALYSIS PERFORMED BY WIRE MANUFACTURER (wt%)

	Specification	Sample
C	0.48 to 0.53	0.49
Mg	0.70 to 0.90	0.77
P	0.040 maximum	0.014
S	0.040 maximum	0.017
Si	0.20 to 0.35	0.30
Cr	0.80 to 1.10	1.08
V	0.15 minimum[a]	0.27
Fe (by difference)	96.54[a] to 97.67	97.06

[a] Assuming 0.50 maximum for V.

[a] New England High Carbon Wire Corporation, Millsbury, Massachusetts 01527.

778 261

VII. REFERENCES

1. United States Nuclear Regulatory Commission, Reactor Safety Research Program, *A Description of Current and Planned Reactor Safety Research Sponsored by the Nuclear Regulatory Commission's Division of Reactor Safety Research*, NUREG-75/058 (June 1975).

2. Argonne National Laboratory, "Mechanical Properties of Zircaloy Containing Oxygen," *Light-Water-Reactor Safety Research Program: Quarterly Progress Report, January-March 1977*, Section III, ANL-77-34 (June 1977).

3. Argonne National Laboratory, "Mechanical Properties of Zircaloy Containing Oxygen," *Light-Water-Reactor Safety Research Program: Quarterly Progress Report, April-June 1977*, Section III, ANL-77-59 (April-June 1977).

4. C. R. Woo (ed.), *Properties of Zircaloy-4 Tubing*, WAPD-TM-585 (December 1966).

DISTRIBUTION RECORD FOR NUREG/CR-0609
(TREE-1331)

Internal Distribution

1 - R. J. Beers, ID

2 - P. E. Litteneker, ID

3-5 - INEL Technical Library

6-10 - Authors

11-50 - Special Internal

External Distribution

51-52 - Saul Levine, Director
Office of Nuclear Regulatory Research, NRC
Washington, D.C. 20555

53-58 - Special External

59-355 - Distribution under R3, Water Reactor Safety Research - Fuel Behavior